A simple rule governs the evolution and development of hominin tooth size

Alistair R. Evans[1,2], E. Susanne Daly[3,4], Kierstin K. Catlett[3,4], Kathleen S. Paul[4,5], Stephen J. King[6], Matthew M. Skinner[7,8], Hans P. Nesse[4], Jean-Jacques Hublin[8], Grant C. Townsend[9], Gary T. Schwartz[3,4] and Jukka Jernvall[10]

[1]School of Biological Sciences, Monash University, VIC 3800, Australia
[2]Geosciences, Museum Victoria, VIC 3001, Australia
[3]Institute of Human Origins, Arizona State University, Tempe, AZ 85287, USA
[4]School of Human Evolution and Social Change, Arizona State University, Tempe, AZ 85287, USA
[5]Center for Bioarchaeological Research, Arizona State University, Tempe, AZ 85287, USA
[6]Department of Anthropology, University of Massachusetts Amherst, Amherst, MA 01003, USA
[7]School of Anthropology and Conservation, University of Kent, Canterbury, CT2 7NR, UK
[8]Department of Human Evolution, Max Planck Institute for Evolutionary Anthropology, Leipzig 04103, Germany
[9]School of Dentistry, The University of Adelaide, South Australia 5005, Australia
[10]Institute of Biotechnology, University of Helsinki 00014, Finland

Abstract

The variation in molar tooth size in humans and our closest relatives (hominins) has strongly influenced our view of human evolution. The reduction in overall size and disproportionate decrease in third molar size have been noted for over a century, and have been attributed to reduced selection for large dentitions due to changes in diet or the acquisition of cooking[1,2]. The systematic pattern of size variation along the tooth row has been described as a 'morphogenetic gradient' in mammal, and more specifically hominin, teeth since Butler[3] and Dahlberg[4]. However, the underlying controls of tooth size have not been well understood, with hypotheses ranging from morphogenetic fields[3] to the clone theory[5]. In this study we address the question: Are there rules that govern how hominin tooth size evolves? Here we propose that the inhibitory cascade, an activator-inhibitor mechanism that affects relative tooth size in mammals[6], produces the default pattern of tooth sizes for all lower primary postcanine teeth (deciduous premolars and permanent molars) in hominins. This configuration is also equivalent to a morphogenetic gradient, at long last pointing to a mechanism that can generate this gradient. The pattern of tooth size remains constant with absolute size in australopiths (including *Ardipithecus*, *Australopithecus* and *Paranthropus*). However, in species of *Homo*, including modern humans, there is a tight link between tooth proportions and absolute size such that a single developmental parameter can explain both the relative and absolute sizes of primary postcanine teeth. Based on the relationship of inhibitory cascade patterning with size, we can use the size at one tooth position to predict the sizes of the remaining four primary postcanine teeth in the row for hominins. Our study provides a development-based expectation to examine the evolution of the unique proportions of human teeth.

Nearly 80 years ago, Butler[3,7] first described the morphogenetic gradient in mammalian postcanine teeth. From anterior to posterior, the deciduous premolars and molars increase in size, and in some species the posterior molars then decrease, with only one local maximum of tooth size along the row. Butler[3] interpreted this pattern to be generated by a morphogenetic field, where the concentration of a diffusible morphogen determined size. The pattern appeared to apply to both deciduous premolars and molars. The deciduous premolars are replaced with a secondary dentition, called the permanent premolars, while the molars are never replaced. Since deciduous premolars and molars are the first teeth to develop at their position in the jaw, they are considered primary teeth[8] and Butler[3] considered them to be part of the same tooth class. While several authors have

investigated the morphogenetic gradient in hominins[4,9], they have generally limited their investigations to permanent premolars rather than their deciduous predecessors.

Kavanagh *et al.*[6] discovered a developmental mechanism controlling relative molar size in mice by experimental manipulation, by either separating adjacent molars or applying growth factors in the culture. In the resulting 'inhibitory cascade' model, molar activator/inhibitor ratio determines the size of subsequently-developing molars. Whereas activation is principally considered to be mesenchymal, previously-initiated molars are the source of inhibition, thereby causing a patterning cascade from anterior to posterior molars. The three molars followed the inhibitory cascade pattern where the second molar was 1/3 of the combined area of all three molars. The pattern appears to explain a high proportion of the variation in relative molar size in murines, primates and mammaliaforms[6,10-15]. Mice lack all premolars and so their patterning cannot be assessed, but the inhibitory cascade implies that a previously-initiated tooth should always inhibit the subsequently-developing tooth (e.g. the fourth deciduous premolar, dp4, should inhibit the first molar, m1).

Here, we test the hypothesis that the inhibitory cascade explains the morphogenetic gradient in the primary postcanine tooth size of hominins and great apes. We divide the lower dentition into sets of three teeth, or triplets: 1) the third and fourth deciduous premolars, dp3 and dp4, and the first molar, m1 (dp3-dp4-m1); 2) dp4-m1-m2, and 3) the three molars (m1-m2-m3). If a triplet follows the inhibitory cascade pattern, then the central tooth is the average size of the two outer teeth. This is mathematically equivalent to the central tooth being 1/3 of the total triplet size (see Supplementary Information). As a result, the three teeth show a linear change in size with tooth position; hence, linearity of size change can be used as a proxy for the inhibitory cascade.

Based on our analysis of between 58 and 66 modern human populations for each molar and 8 populations for deciduous premolars, the average sizes of the first triplet of the human lower postcanine tooth row increase linearly from dp3 through dp4 to m1 (OLS regression $R^2 = 0.9998$; Fig. 1). The third triplet (molars) also follows the inhibitory cascade pattern, but here size is linearly decreasing from m1 to m3 ($R^2 = 0.974$). Therefore, m1 is on average the largest tooth in the row, with size first increasing and then decreasing about this central tooth position. Because the middle tooth is the largest, the second triplet does not follow the linear pattern predicted by the inhibitory cascade. We can describe this change in direction as a *reversal* of the inhibitory cascade patterning, reaffirming Butler's[3] morphogenetic gradient.

Fourteen species of fossil hominins (eight of which include metrics for both deciduous premolars) also follow the inhibitory cascade in the first triplet (Fig. 1; Extended Data Fig. 1). However, in all fossil hominins the second or third molar is the largest tooth on average. In most australopiths (e.g. *Paranthropus boisei*; Fig. 1) the second triplet dp4-m1-m2 also follows the inhibitory cascade such that central tooth (m1) size is the average of the two adjacent teeth, pushing the reversal position to m2 or m3. This contrasts with a reversal position at m1 in *Homo sapiens*. The close fit of the dp3-dp4-m1 triplet for all hominin species allows us to predict that the average size of the undiscovered dp4 of *Ardipithecus ramidus* will be the average of the dp3 and m1 sizes, i.e. 73 mm^2 in area (star in Fig. 1a).

If the relative size of each tooth in a row is expressed as a proportion of the largest tooth in the row, then a close relationship between absolute m1 size and relative tooth size is revealed for species in the genus *Homo* (Extended Data Fig. 2). This contrasts with the remaining hominin taxa (i.e., the australopiths), where the proportions are essentially constant with m1 size. Ape tooth proportions are intermediate to *Homo* species and australopiths.

In a 3-dimensional plot combining tooth position, the relative size of each tooth, and the absolute size of m1, all data points generally fall on two distinct planes in 3D space (i.e. relative size has linear relationships with both variables; Extended Data Fig. 3; Supplementary Movies 1 and 2). For *Homo*, the deciduous premolars and first molars fall on the first plane, Plane A, while the other molars fall close to the second plane, Plane B (average deviations from Plane A and B are 0.046 and 0.026, respectively; Extended Data Fig. 3a). The intersection of these two planes represents the position of the reversal of the inhibitory cascade, where tooth size changes from increasing to decreasing. In *Homo*, the reversal shifts from m2 to m1 when m1 size decreases. In

contrast, in australopiths, the first four primary teeth (dp3, dp4, m1 and m2) all fall on Plane A, and m2 and m3 fall on Plane B (average deviations from Plane A and Plane B are 0.036 and 0.022, respectively; Extended Data Fig. 3b), and the reversal remains at m2. Tooth sizes for great apes also fall on two planes in 3D space in similar positions to those of hominins (Extended Data Fig. 3c,d).

The tight fit to both Planes A and B indicates two important findings: 1) that these species follow the expected inhibitory cascade pattern of linear change for the first three (or four) teeth in the primary tooth row; 2) that there is a strong relationship between tooth position and proportional sizes in all hominins. However, in the genus *Homo* the reversal position changes with absolute m1 size, while in the australopiths the reversal position is unaffected by absolute m1 size. The tight correspondence of the largest tooth in the row to m1 size (R^2 = 0.90 for both *Homo* and australopiths; Extended Data Fig. 4) allows us to convert proportional size to absolute size based on a given m1 size (see Supplementary Information for calculations). Standardizing m1 size to a straight line in 3D space produces 3D surfaces that can be used to represent primary postcanine tooth sizes for either australopiths or *Homo* species (Fig. 2). This diagram essentially shows how absolute tooth sizes and proportions vary with change in m1 size. Deviations of the species means from these surfaces are relatively minor (average and maximum deviation for *Homo* species are 7.1% and 18.0% respectively; for australopiths, 7.6% and 24.5%; see Extended Data Fig. 5).

Supplementary Spreadsheet 1 predicts the sizes of the full tooth row based on a given tooth position and size. These sizes are predictions based on species means and interspecific scaling relationships, and so represent sizes and proportions typical of species for that m1 size. The 3D prediction surfaces are represented as a contour plot in Fig. 3, with different contours for *Homo* species and australopiths, showing the sizes at each tooth position for a given m1 size in that row (see also Extended Data Fig. 6). The predicted absolute sizes of all teeth for three hominin m1 sizes are shown in Fig. 3b. This diagram also illustrates which tooth triplets follow the inhibitory cascade and where the inhibitory cascade pattern reverses along the tooth row (asterisks) according to the intersection of the planes in Extended Data Fig. 3.

Given the close fit of almost all australopiths to their prediction surface (Fig. 2) and a very similar pattern in the great apes, we postulate that a tight association between tooth proportions and m1 size existed at the base of the hominin clade (Extended Data Figs 1-3). Near the origin of the genus *Homo*, it appears that there was an alteration of the scaling relationship between m1 size and inhibitory cascade patterning, such that the reversal position changes with absolute m1 size (Fig. 4). In fact, *Homo habilis* shows more similar proportions to australopiths than its congeners, which suggests this shift occurred after the origin of *H. habilis*, and perhaps reallocation of *H. habilis* to the genus *Australopithecus* is warranted[16]. However, this conclusion is based on a limited sample (Supplementary Information). Heterogeneity in the early *Homo* pattern is also present in the Dmanisi specimens – one specimen (D2600) is closer to the australopiths whereas the others are closer to the *Homo* pattern (Supplementary Information).

Interestingly, the smallest-bodied hominin, *H. floresiensis*, is most similar to the smallest-bodied great ape, *P. paniscus*, in tooth sizes and proportions and are smaller in comparison to tooth rows of human populations with the largest tooth at m2 (Extended Data Fig. 1). Among fossil hominins, *H. floresiensis* has proportions similar to *Homo heidelbergensis* and *Homo erectus*, but ~40% smaller in area. As expected, the recently described australopith, *Australopithecus deyiremeda*[17], and the late surviving *Australopithecus sediba* both follow the australopith pattern.

Homo sapiens demonstrate a similar pattern to other species of *Homo* but at smaller m1 sizes, producing disproportionately decreased third molars. While the overall pattern in modern humans is for the largest tooth to be at m1, in contrast to m2 or m3 in fossil hominins, a reasonable proportion of humans have the second molar as the largest tooth (11 to 19% of individuals in some populations[18], and 8.6% of the population means in our sample).

We note that specimen-level predictions can show deviation from the species-level scaling patterns. For example, when the size of each tooth is used to predict the sizes of the other teeth in the same specimen, the average error is 10.3% and 7.9% for *Homo* and australopiths respectively (Supplementary Information). The largest prediction errors (above 30%) are found in *H. erectus*

(D211, Thomas I), *H. heidelbergensis* (Arago 1) and *H. neanderthalensis* (KMH1, Krapina 1,7,79 and Krapina 64). Some of the discrepancies are likely from errors in size estimation due to developmental age, preservation and wear, and potentially identification inaccuracies in making composite specimens. Increased intraspecific variation in *Homo* species could also result from relaxed selection or multiple selection pressures. Relaxed selection is implicated by the increased fluctuating asymmetry found in most *Homo* dentitions compared to australopiths and great apes[19,20]. Yet another possibility is developmental instability when molars approach equal size, as, for example, extra molar presence in mouse experiments appears to be linked to the molars being of equal size[6].

Here we used a simple measure of tooth size, length by width rectangular area, because it is the most commonly used and, therefore, extensive data sets are available. To assess alternative measures of size we calculated three additional metrics from microCT scans using a subset of fossil hominin specimens: tooth occlusal outline area, enamel-dentine junction 3D surface area, and cervical cross-sectional area (Fig. 1b). All show the same general pattern of size relationships (Extended Data Fig. 7). The first two of these were very highly correlated with rectangular area ($R^2 > 0.94$), cervical area only slightly less so ($R^2 = 0.86$; Extended Data Fig 8).

Developmentally, in the activator-inhibitor model, higher relative inhibition yields smaller posterior molars and lower relative inhibition larger posterior molars. However, absolute tooth size was essentially independent of the slope of the inhibitory cascade studied in the mouse-derived model (position along the inhibitory axis[6]; Extended Data Fig. 9). In contrast, hominins appear to follow a simpler pattern: in australopiths, the inhibitory cascade pattern remains constant with changing m1 size in australopiths, while in *Homo*, there is a link between the proportions and absolute m1 size (Extended Data Fig. 2). The simplest and fastest way to modify both proportions and size should be through changes in the activation of the first tooth because the first tooth in a developmental series is unimpeded by the inhibition of other teeth. We hypothesize a decrease in mesenchymal activation and the maintenance of inhibition drives the change in tooth proportions in *Homo*. The mechanism controlling reversal position, however, remains to be determined. While the inhibitory cascade has been invoked to account for patterns in vertebrate limbs, digits, and somites[21], it remains to be tested whether absolute and relative size could be linked across multiple vertebrate systems.

In conclusion, previous work comparing relative molar sizes using step indices[22] and ratios[23] identified significant changes in these proportions throughout hominin evolution; here we explain such changes based on the developmental inhibitory cascade mechanism. Typically, palaeoanthropologists have emphasised function, such as changing bite force, to explain the variation in both hominin and great ape tooth proportions[24-27]. While functionally-based scenarios may give a reason for reduced posterior tooth size in hominin evolution, they cannot account for the developmentally-based phenomenon of the primary teeth always following the inhibitory cascade patterning. While selective pressures can be used to explain the general evolutionary result, only by including development can one explain the detailed manner by which it was achieved. As well as providing a development-based expectation for the evolution of the hominin dentition, the inhibitory cascade and its scaling with tooth size hold promise for evolutionary anthropology. In essence, an activator-inhibitor framework allows the prediction of the whole pattern from a single constituent, demonstrating human evolutionary developmental biology as a predictive science.

Methods

Tooth size data. Human lower primary postcanine tooth sizes, defined as rectangular areas of mesiodistal length × maximum buccolingual width, were collated from the literature, and measured from dental casts at the Burlington Growth Centre, Toronto, Canada. Population-level means of molar sizes were collated from studies where all three molars were measured and wear was not excessive, largely from compilations[23,28] (see Supplementary Information). Fossil hominin tooth

size measurements were compiled at the specimen level and assigned to taxonomic groups (see Supplementary Information), using measurements adjusted for wear when available. *Homo erectus* specimens from Asia and Africa were grouped separately. Ape tooth size measurements were obtained from the literature[29] or measured from museum specimens (see Supplementary Information). For all individual-level data, measurements taken from both sides of the same individual were averaged. Individuals of the same sex were averaged, then sexes were averaged to obtain a population or species mean size for each tooth.

Analyses. For each primary tooth row (mean of sex, population or species), all teeth were scaled so that the largest tooth in the row equalled 1, called *Prop Max in Row*. For hominins and great apes separately, we used R v. 3.1.3[30] to carry out multiple linear regression for *Prop Max in Row ~ Tooth Position + Area of m1*, and linear regression for *Max Area in Row ~ Area of m1*. For hominins, *Prop Max in Row* was converted to *Area* by multiplying it by *Max Area in Row* for the given m1 size. This function was then divided by the ratio of the expected *Area of m1* to that calculated for m1 to give m1 size a 1:1 relationship with *Area* in the predictive surface (see Supplementary Information for calculations). Individual-level fossil data were used for the prediction error calculation using the relevant *Homo* or australopith prediction surface. Prediction error was calculated as 100×|(observed - predicted)|/observed.

3D tooth size data. X-ray microtomographic scans of six hominin specimens with three sufficiently unworn lower molars were carried out at the Max Planck Institute for Evolutionary Anthropology, Leipzig, Germany. 3D tooth models were measured for rectangular area, tooth occlusal outline area, enamel-dentine junction 3D surface area, and cervical cross-sectional area (Fig. 1b).

1 Brace, C. L. Environment, tooth form, and size in the Pleistocene. *J. Dent. Res.* **46**, 809-816, (1967).
2 Bermúdez de Castro, J. M. & Nicolas, M. E. Posterior dental size reduction in hominids: the Atapuerca evidence. *Am. J. Phys. Anthropol.* **96**, 335-356, (1995).
3 Butler, P. M. Studies of the mammalian dentition. Differentiation of the post-canine dentition. *P. Roy. Soc. Lond. B Bio.* **109**, 1-36, (1939).
4 Dahlberg, A. A. The changing dentition of man. *J. Am. Dent. Assoc.* **32**, 676-690, (1945).
5 Osborn, J. W. in *Development, Function and Evolution of Teeth* (eds P.M. Butler & K.A. Joysey) 171-201 (Academic Press, 1978).
6 Kavanagh, K. D., Evans, A. R. & Jernvall, J. Predicting evolutionary patterns of mammalian teeth from development. *Nature* **449**, 427-432, (2007).
7 Butler, P. M. Studies of the mammalian dentition: I. The teeth of *Centetes ecaudatus* and its allies. *P. Roy. Soc. Lond. B Bio.* **107**, 103-132, (1937).
8 Owen, R. *Odontography*. (Hippolyte Bailliere, 1840-1845).
9 Townsend, G. C. & Brown, T. Morphogenetic fields within the dentition. *Aust. Orthod. J.* **7**, 3-12, (1981).
10 Polly, P. D. Evolutionary biology - Development with a bite. *Nature* **449**, 413-415, (2007).
11 Renvoisé, E. *et al.* Evolution of mammal tooth patterns: new insights from a developmental prediction model. *Evolution* **63**, 1327-1340, (2009).
12 Wilson, L. A. B., Madden, R. H., Kay, R. F. & Sanchez-Villagra, M. R. Testing a developmental model in the fossil record: molar proportions in South American ungulates. *Paleobiology* **38**, 308-321, (2012).
13 Bernal, V., Gonzalez, P. N. & Ivan Perez, S. Developmental processes, evolvability, and dental diversification of New World monkeys. *Evolutionary Biology* **40**, 532-541, (2013).
14 Halliday, T. J. D. & Goswami, A. Testing the inhibitory cascade model in Mesozoic and Cenozoic mammaliaforms. *BMC Evol. Biol.* **13**, (2013).
15 Schroer, K. & Wood, B. Modeling the dental development of fossil hominins through the inhibitory cascade. *J. Anat.* **226**, 150-162, (2015).
16 Wood, B. & Collard, M. The human genus. *Science* **284**, 65-71, (1999).

17 Haile-Selassie, Y. *et al.* New species from Ethiopia further expands Middle Pliocene hominin diversity. *Nature* **521**, 483-488, (2015).
18 Garn, S. M., Kerewsky, R. S. & Lewis, A. B. Molar size sequences and fossil taxonomy. *Science* **142**, 1060, (1963).
19 Kieser, J. A. & Groeneveld, H. T. The assessment of fluctuating odontometric asymmetry from incomplete hominid fossil data. *Anthropologischer Anzeiger* **44**, 175-182, (1986).
20 Kegley, A. D. T. & Hemingway, J. in *Voyages in Science: essays by South African anatomists in honour of Phillip V. Tobias' 80th birthday* (eds G. Strkalj, N. Pather, & B. Kramer) 35-49 (Content Solutions, 2005).
21 Young, N. M., Winslow, B., Takkellapati, S. & Kavanagh, K. Shared rules of development predict patterns of evolution in vertebrate segmentation. *Nat. Commun.* **6**, (2015).
22 Selmer-Olsen, R. An odontometrical study on the Norwegian Lapps. *Skrift Norske Vidensk-Akademi* **3**, 1-167, (1949).
23 Wolpoff, M. H. Metric trends in hominid dental evolution. *Case Western Reserve University Studies in Anthropology* **2**, (1971).
24 Lucas, P. W. *Dental Functional Morphology*. (Cambridge University Press, 2004).
25 Greaves, W. S. The jaw lever system in ungulates: a new model. *J. Zool.* **184**, 271-285, (1978).
26 Spencer, M. A. Force production in the primate masticatory system: electromyographic tests of biomechanical hypotheses. *J. Hum. Evol.* **34**, 25-54, (1998).
27 Lucas, L. *Variation in Dental Morphology and Bite Force Along the Tooth Row in Anthropoids* PhD thesis, Arizona State University, (2012).
28 Kieser, J. A. *Human Adult Odontometrics*. (Cambridge University Press, 1990).
29 Johanson, D. C. Some metric aspects of the permanent and deciduous dentition of the pygmy chimpanzee (*Pan paniscus*). *Am. J. Phys. Anthropol.* **41**, 39-48, (1974).
30 R Development Core Team. *R: A Language and Environment for Statistical Computing*. (R Foundation for Statistical Computing, 2015).
31 Dembo, M., Matzke, N. J., Mooers, A. O. & Collard, M. Bayesian analysis of a morphological supermatrix sheds light on controversial fossil hominin relationships. *Proceedings of the Royal Society B* **282**, (2015).
32 Faraway, J. *Linear Models with R*. (Chapman & Hall/CRC, 2005).
33 Schrago, C. G. & Voloch, C. M. The precision of the hominid timescale estimated by relaxed clock methods. *Journal of Evolutionary Biology* **26**, 746-755, (2013).
34 Stone, A. C. *et al.* More reliable estimates of divergence times in *Pan* using complete mtDNA sequences and accounting for population structure. *Philosophical Transactions of the Royal Society B* **365**, 3277-3288, (2010).
35 Axelsson, G. & Kirveskari, P. Crown size of permanent teeth in Icelanders. *Acta Odontol. Scand.* **41**, 181-186, (1983).
36 Axelsson, G. & Kirveskari, P. Crown size of deciduous teeth in Icelanders. *Acta Odontol. Scand.* **42**, 339-343, (1984).
37 Dahlberg, A. A. The dentition of the first agriculturists (Jarmo, Iraq). *Am. J. Phys. Anthropol.* **18**, 243-256, (1960).
38 Kaul, V. & Prakash, S. Crown dimensions of deciduous and permanent teeth of Jats from Haryana (India). *Ann. Hum. Biol.* **11**, 351-354, (1984).
39 Margetts, B. & Brown, T. Crown diameters of deciduous teeth in Australian Aboriginals. *Am. J. Phys. Anthropol.* **48**, 493-502, (1978).
40 Townsend, G. C. & Brown, T. Tooth size characteristics of Australian Aborigines. *Occasional Papers in Human Biology* **1**, 17-38, (1979).
41 Moyers, R. E., van der Linden, F. P. G. M., Riolo, M. L. & McNamara, J. A., Jr. *Standards of Human Occlusal Development*. 371 (Center for Human Growth and Development, University of Michigan, 1976).
42 Paul, K. S. This study.

43 Sciulli, P. W. Evolution of dentition in prehistoric Ohio Valley Native Americans III. Metrics of deciduous dentition. *Am. J. Phys. Anthropol.* **116**, 140-153, (2001).
44 Sciulli, P. W. Size and morphology of the permanent dentition in prehistoric Ohio Valley Amerindians. *Am. J. Phys. Anthropol.* **50**, 615-628, (1979).
45 Townsend, G. C. Tooth size in children and young adults with trisomy 21 (Down) syndrome. *Arch. Oral Biol.* **28**, 159-166, (1983).
46 Moss, M. L., Chase, P. S. & Howes, R. I. Comparative odontometry of permanent post-canine dentition of American whites and negroes. *Am. J. Phys. Anthropol.* **27**, 125-142, (1967).
47 Jacobson, A. *The Dentition of the South African Negro*. (Higginsbotham, 1982).
48 Barnes, D. S. Tooth morphology and other aspects of the Teso dentition. *Am. J. Phys. Anthropol.* **30**, 183-194, (1969).
49 Calcagno, J. M. Dental reduction in Post-Pleistocene Nubia. *Am. J. Phys. Anthropol.* **70**, 349-363, (1986).
50 van Reenen, J. F. Dental features of a low-caries primitive population. *J. Dent. Res.* **45**, 703-713, (1966).
51 Drennan, M. R. The dentition of a Bushman tribe. *Annls S. Afr. Mus.* **24**, 61-87, (1929).
52 van Reenen, J. F. in *Teeth: Form, Function and Evolution* (ed B. Kurtén) 182-203 (Columbia University Press, 1982).
53 Greene, D. L., Ewing, G. H. & Armelago, G. J. Dentition of a Mesolithic population from Wadi Halfa, Sudan. *Am. J. Phys. Anthropol.* **27**, 41-56, (1967).
54 Hosaka, T. Statistische Untersuchungen über die Zähne bei Chinesen mit besonderer Berücksichtigung der Rassenunterschiede. *Journal of Oriental Medicine* **24**, 1065–1090, 1230–1251; 10**25**: 1348–1368, (1936).
55 Brace, C. L. Tooth reduction in the Orient. *Asian Perspect.* **19**, 203-219, (1976).
56 Dutta, P. C. An odontometric analysis of molar crown characters of Bronze Age Harappans. *Anthropologischer Anzeiger* **41**, 67-72, (1983).
57 Lukacs, J. R. Tooth size variation in prehistoric India. *Am. Anthropol.* **87**, 811-825, (1985).
58 Walimbe, S. R. in *Dental Anthropology: Applications and Methods* (ed V.R. Reddy) 332-332 (Inter-India Publications, 1985).
59 Sharma, J. C. & Kaul, V. Dental morphology and odontometry in Panjabis. *Journal of the Indian Anthropological Society* **12**, 213-226, (1977).
60 Jacob, T. Racial identification of Bronze Age human dentitions from Bali, Indonesia. *J. Dent. Res.* **46**, 903-910, (1967).
61 Brace, C. L. & Nagai, M. Japanese tooth size: past and present. *Am. J. Phys. Anthropol.* **59**, 399-411, (1982).
62 Yamada, E. The anthropological study of the Japanese teeth. *J. Nippon Dent. Ass.* **25**, 15-46, 101-132, 177-208, 255-286, 329-344, 450-481, 528-560, 609-656, 710-714, 774-812, (1932).
63 Mijsberg, W. A. On sexual differences in the teeth of Japanese. *Koninklijke Akademie voor Wetenschap* **34**, 1111, (1931).
64 Sharma, J. C. Dental morphology and odontometry of the Tibetan immigrants. *Am. J. Phys. Anthropol.* **61**, 495-505, (1983).
65 Smith, P., Brown, T. & Wood, W. B. Tooth size and morphology in a recent Australian Aboriginal Population from Broadbeach, South East Queensland. *Am. J. Phys. Anthropol.* **55**, 423-432, (1981).
66 Freedman, L. & Lofgren, M. Odontometrics of Western Australian Aborigines. *Archaeol. Ocean.* **16**, 87-93, (1981).
67 Barrett, M. J., Brown, T. & MacDonald, M. R. Dental observations on Australian Aborigines: MD crown diameters of permanent teeth. *Aust. Dent. J.* **8**, 150-156, (1963).
68 Barrett, M. J., Brown, T., Arato, G. & Ozols, I. V. Dental observations on Australian Aborigines: BL diameters of deciduous and permanent teeth. *Aust. Dent. J.* **9**, 280-285, (1964).
69 Kirveskari, P., Hansson, H., Hedegard, B. & Karlsson, U. Crown size and hypodontia in permanent dentition of modern Skolt Lapps. *Am. J. Phys. Anthropol.* **48**, 107-112, (1978).

70 Mayhall, J. T. The dental morphology of the Inuit of the Canadian Central Arctic. *Ossa* **6**, 199-218, (1979).
71 Moorrees, C. F. A. *The Aleut Dentition*. (Harvard University Press, 1957).
72 Perzigian, A. J. The dentition of Indian Knoll skeletal population: odontometrics and cusp number. *Am. J. Phys. Anthropol.* **44**, 113-121, (1976).
73 Nelson, C. T. The teeth of the Indians of Pecos Pueblo. *Am. J. Phys. Anthropol.* **23**, 261-293, (1938).
74 Hinton, R. J., Smith, M. O. & Smith, F. H. Tooth size changes in prehistoric Tennessee Indians. *Hum. Biol.* **52**, 229-245, (1980).
75 Bailit, H. L., Dewitt, S. J. & Leigh, R. A. The size and morphology of Nasioi dentition. *Am. J. Phys. Anthropol.* **28**, 271-288, (1968).
76 Stein, M. R. & Epstein, J. L. The molar teeth of New Britain Melanesians. *J. Am. Dent. Assoc.* **21**, 1409-1413, (1934).
77 Turner, C. G. & Swindler, D. R. The dentition of New Britain West Nakanai Melanesians VIII Peopling of the Pacific. *Am. J. Phys. Anthropol.* **49**, 361-371, (1978).
78 Doran, G. A. & Freedman, L. Metrical features of dentition and arches of populations from Goroka and Lufa, Papua New Guinea. *Hum. Biol.* **46**, 583-594, (1974).
79 Kieser, J. A., Groeneveld, H. T. & Preston, C. B. An odontometric analysis of the Lengua Indian dentition. *Hum. Biol.* **57**, 611-620, (1985).
80 Scott, E. C. Increase of tooth size in prehistoric coastal Peru, 10,000 BP-1,000 BP. *Am. J. Phys. Anthropol.* **50**, 251-258, (1979).
81 White, T. D., Suwal, G. & Asfawi, B. *Australopithecus ramidus*, a new species of early hominid from Aramis, Ethiopia. *Nature* **371**, 306-312, (1994).
82 Semaw, S. *et al.* Early Pliocene hominids from Gona, Ethiopia. *Nature* **433**, 301-305, (2005).
83 Hill, A. Early hominid from Baringo, Kenya. *Nature* **315**, 222-224, (1985).
84 Johanson, D. C., White, T. D. & Coppens, Y. Dental remains from the Hadar Formation, Ethiopia: 1974–1977 collections. *Am. J. Phys. Anthropol.* **57**, 545-603, (1982).
85 Kimbel, W. H., Johanson, D. C. & Rak, Y. The first skull and other new discoveries of *Australopithecus afarensis* at Hadar, Ethiopia. *Nature* **368**, 449-451, (1994).
86 White, T. D. New fossil hominids from Laetolil, Tanzania. *Am. J. Phys. Anthropol.* **46**, 197–229, (1977).
87 White, T. D., Suwa, G., Simpson, S. & Asfaw, B. Jaws and teeth of *Australopithecus afarensis* from Maka, Middle Awash, Ethiopia. *Am. J. Phys. Anthropol.* **111**, 45-68, (2000).
88 Grine, F. E. A new juvenile hominid (Mammalia: Primates) from Member 3, Kromdraai Formation, Transvaal, South Africa. *Transvaal Museum Memoirs* **33** 165-239, (1982).
89 Grine, F. E. *The deciduous dentition of the Kalahari San, the South African negro and the South African Plio-Pleistocene hominids*, University of the Witwatersrand, (1984).
90 Robinson, J. T. *The dentition of the Australopithecinae*. (Transvaal Museum, 1956).
91 Grine, F. E. A new composite juvenile specimen of *Australopithecus africanus* (Mammalia, Primates) from Member 4 Sterkfontein Formation, Transvaal. *Annls S. Afr. Mus.* **84**, 169-201, (1981).
92 Haile-Selassie, Y., Saylor, B. Z., Deino, A., Alene, M. & Latimer, B. M. New hominid fossils from Woranso-Mille (Central Afar, Ethiopia) and taxonomy of early *Australopithecus*. *Am. J. Phys. Anthropol.* **141**, 406-417, (2010).
93 Coffing, K., Feibel, C., Leakey, M. & Walker, A. Four-million-year-old hominids from East Lake Turkana, Kenya. *Am. J. Phys. Anthropol.* **93**, 55-65, (1994).
94 Ward, C., Leakey, M. & Walker, A. Morphology of *Australopithecus anamensis* from Kanapoi and Allia Bay, Kenya. *J. Hum. Evol.* **41**, 255-368, (2001).
95 Leakey, M. G., Feibel, C. S., McDougall, I., Ward, C. & Walker, A. New specimens and confirmation of an early age for *Australopithecus anamensis*. *Nature* **393**, 62-66, (1998).
96 Berger, L. R. *et al. Australopithecus sediba*: A new species of Homo-like australopith from South Africa. *Science* **328**, 195-204, (2010).

97 Gabunia, L. & Vekua, A. A Plio-Pleistocene hominid from Dmanisi, East Georgia, Caucasus. *Nature* **373**, 509-512, (1995).
98 Macaluso, P. J. J. Variation in dental remains from Dmanisi, Georgia. *Anthropol. Sci.* **118**, 31-40, (2010).
99 Wu, X. & Poirier, F. E. *Human evolution in China: a metric description of the fossils and a review of the sites*. (Oxford University Press New York, 1995).
100 Zanolli, C. *et al.* Brief communication: two human fossil deciduous molars from the Sangiran Dome (Java, Indonesia): outer and inner morphology. *Am. J. Phys. Anthropol.* **147**, 472-481, (2012).
101 Roebroeks, W. Updating the earliest occupation of Europe. *Curr. Anthropol.* **35**, 301-305, (1994).
102 Howell, F. C. European and northwest African middle Pleistocene hominids. *Curr. Anthropol.* **1**, 195-232, (1960).
103 Grine, F. E. Comparison of the deciduous dentitions of African and Asian hominids. *Cour. Foursch. Inst. Senckenberg* **69**, 69-82, (1984).
104 Weidenreich, F. The dentition of *Sinanthropus pekinensis*: a comparative odontography of the hominids. *Palaeontogia Sinica, New Series D* **1 (Whole Series 101)**, 1-180, (1937).
105 Leakey, R. & Walker, A. Further hominids from the Plio-Pleistocene of Koobi Fora, Kenya. *Am. J. Phys. Anthropol.* **67**, 135-163, (1985).
106 Leakey, R. & Wood, B. New evidence of the genus *Homo* from East Rudolf, Kenya. II. *Am. J. Phys. Anthropol.* **39**, 355-368, (1973).
107 Brown, F., Harris, J., Leakey, R. & Walker, A. Early *Homo erectus* skeleton from west Lake Turkana, Kenya. *Nature* **316**, 788-792, (1985).
108 Rightmire, G. Middle Pleistocene hominids from Olduvai Gorge, northern Tanzania. *Am. J. Phys. Anthropol.* **53**, 225-241, (1980).
109 Arambourg, C. Le gisement de Ternifine II. L'Atlanthropus mauritanicus. *Archives de L'Institute de Paleontologie Humaine* **32**, 37-190, (1963).
110 Bermúdez de Castro, J. M. Dental remains from Atapuerca (Spain) I. metrics. *J. Hum. Evol.* **15**, 265-287, (1986).
111 Sausse, F. La mandibule de la carrière Thomas I (Casablanca). *Anthropologie* **79**, 81-112, (1975).
112 Morwood, M. J. *et al.* Further evidence for small-bodied hominins from the Late Pleistocene of Flores, Indonesia. *Nature* **437**, 1012-1017, (2005).
113 Tobias, P. V. *The Skulls, Endocasts, and Teeth of Homo Habilis: pt. 1-4*. Vol. 4 (Cambridge University Press, 1991).
114 de Lumley, M. A. in *La Grotte de l'Hortus (Valflaunes-Herault) Etudes Quaternaires, Mémoire no. 1* 375-385 (Laboratoire de paléontologie humaine et de préhistoire, Université de Provence, 1972).
115 Mallegni, F. & Ronchitelli, A. Deciduous teeth of the Neandertal mandible from Molare Shelter, near Scario (Salerno, Italy). *Am. J. Phys. Anthropol.* **79**, 475-482, (1989).
116 Sakura, H. in *The Amud Man and His Cave Site* (eds H. Suzuki & F. Takai) 207-229 (University of Tokyo, 1970).
117 Ascenzi, A. & Sergre, A. A new Neandertal child mandible from an Upper Pleistocene site in southern Italy. *Nature* **233**, 280-283, (1971).
118 Faerman, M., Zilberman, U., Smith, P., Kharitonov, V. & Batsevitz, V. A Neanderthal infant from the Barakai Cave, Western Caucasus. *J. Hum. Evol.* **27**, 405–415, (1994).
119 Toussaint, M. *et al.* The Neandertal lower right deciduous second molar from Trou de l'Abîme at Couvin, Belgium. *J. Hum. Evol.* **58**, 56-67, (2010).
120 Arsuaga, J. *et al.* The human remains from Cova Negra (Valencia, Spain) and their place in European Pleistocene human evolution. *J. Hum. Evol.* **18**, 55-92, (1989).

121 Mizoguchi, Y. in *Neanderthal Burials. Excavations of the Dederiyeh Cave, Afrin, Syria.* (eds T Akazawa & S Muhesen) 221-262 (International Research Center for Japaneses Studies, 2002).
122 Kondo, O. & Ishida, H. in *Neanderthal Burials. Excavations of the Dederiyeh Cave, Afrin, Syria.* (eds T Akazawa & S Muhesen) 323-335 (International Research Center for Japaneses Studies, 2002).
123 Tillier, A.-M. Le crâne d'enfant d'Engis 2: un exemple de distribution des caractères juvéniles primitifs et néanderthaliens. *Bull. Soc. Roy. Belge Anthrop. Prehist.* **94**, 51-76, (1983).
124 de Lumley, M.-A. & Giacobini, G. Les néandertaliens de la Caverna delle Fate (Finale Ligure, Italie). II–Les dents. *L'Anthropologie* **117**, 305-344, (2013).
125 Tillier, A.-M. & Genet-Varcin, E. La plus ancienne mandibule d'enfant découverte en France dans le gisement de La Chaise de Vouthon (Abri Suard) en Charente. *Zeitschrift für Morphologie und Anthropologie*, 196-214, (1980).
126 Tillier, A.-M. La dentition de l'enfant moustérien Chateauneuf 2 découvert à l'abri de Hauteroche (Charente). *L'Anthropologie* **83**, 417-438, (1979).
127 Tillier, A.-M. Les enfants néanderthaliens de Devil's Tower (Gibraltar). *Zeitschrift für Morphologie und Anthropologie*, 125-148, (1982).
128 Tillier, A.-M., Hardy, M., David, F., Girard, M. & d'Iatchenko, V. À propos de deux molaires déciduales inférieures provenant des niveaux moustériens de la Grotte du Bison (Arcy-sur-Cure, Yonne, France). Un exemple de lésion cervicale inédite chez un enfant néanderthalien. *PALEO. Revue d'archéologie préhistorique* **24**, 271-278, (2013).
129 Bailey, S. E. & Hublin, J.-J. Dental remains from the Grotte du Renne at Arcy-sur-Cure (Yonne). *J. Hum. Evol.* **50**, 485-508, (2006).
130 de Lumley, M. A. *Anténéandertaliens et Néandertaliens du Bassin méditerranéen occidental européen*. (Laboratoire de paléontologie humaine et de préhistoire, Université de Provence, 1973).
131 Tillier, A.-M., Vandermeersch, B., Arensburg, B. & Chech, M. New human remains from Kebara Cave (Mount Carmel). The place of the Kebara hominids in the Levantine Mousterian fossil record. *Paléorient* **29**, 35-62, (2003).
132 Wolpoff, M. H. The Krapina dental remains. *Am. J. Phys. Anthropol.* **50**, 67-113, (1979).
133 Heim, J. L. *Les enfants néandertaliens de la Ferrassie*. (Fondation Singer Polignac. Masson, 1982).
134 Henry-Gambier, D., Maureille, B. & White, R. Vestiges humains des niveaux de l'Aurignacien ancien du site de Brassempouy (Landes). *Bull. Mém. Soc. Anthropol. Paris* **16**, 49–87, (2004).
135 Madre-Dupouy, M. *L'enfant du Roc de Marsal: étude analytique et comparative*. (Editions du Centre National de la Recherche Scientifique, 1992).
136 Ferembach, D. Les ossements humains de Salemas (Portugal). *Communicoes Servs. Geol. Port.* **48**, 165-185, (1964).
137 Trinkaus, E. Dental remains from the Shanidar adult Neanderthals. *J. Hum. Evol.* **7**, 369-382, (1978).
138 Trinkaus, E. *The Shanidar Neandertals*. (Academic Press New York, 1983).
139 McCown, T. D. & Keith, A. *The Stone Age of Mount Carmel. The Fossil Human Remains from the Levalloiso-Mousterian, volume II*. (Clarendon Press, 1939).
140 Gremiatski, M. A. in *Teshik-Tash, l'homme paleolithique* (eds M.A. Gremiatski & M.F. Nesturkh) 137-187 (Trudy Uzkekist. Fil. Akad. Nauk SSSR, 1949).
141 Day, M., Leakey, R., Walker, A. & Wood, B. New hominids from East Turkana, Kenya. *Am. J. Phys. Anthropol.* **45**, 369-435, (1976).
142 Leakey, R. E. Further evidence of lower pleistocene hominids from East Rudolf, North Kenya. *Nature* **231**, 241-245, (1971).
143 Keyser, A. W., Menter, C. G., Berger, L., Moggi-Cecchi, J. & Pickering, T. R. Drimolen: a new hominind-bearing site in Gauteng, South Africa. *S. Afr. J. Sci.* **96**, 193-197, (2000).

144 Keyser, A. The Drimolen skull: the most complete australopithecine cranium and mandible to date. *S. Afr. J. Sci.* **96**, 189-193, (2000).
145 Brain, C. New finds at the Swartkrans Australopithecine site. *Nature* **225**, 1112-1119, (1970).
146 Grine, F. E. in *Swartkrans: A Cave's Chronicle of Early Man Transvaal Museum Monograph 8* (ed C.K. Brain) 75-116 (Transvaal Museum, 1993).
147 Grine, F. E. & Daegling, D. J. New mandible of *Paranthropus robustus* from Member 1, Swartkrans Formation, South Africa. *J. Hum. Evol.* **24**, 319 - 333, (1993).
148 Grine, F. E. *Evolutionary History of the"Robust" Australopithecines*. (Aldine de Gruyter, 1988).
149 Grine, F. E. New hominid fossils from the Swartkrans Formation (1979-1986 excavations): craniodental specimens. *Am. J. Phys. Anthropol.* **79**, 409-449, (1989).
150 King, S. J. This study.
151 Catlett, K. K. & Daly, E. S. This study.

Supplementary Information is available in the online version of the paper.

Acknowledgements This contribution is dedicated to the late Prof. Percy Butler, the inspiration for much of this work and discoverer of the morphogenetic gradient in teeth, who unfortunately did not see this work completed. We thank Mikael Fortelius, Gudrun Evans, Ai-Ling Khoo, Fred Grine, Peter Trusler, Justin Adams, Julie Clutterbuck, Lap Chieu, David Hocking, Matthew McCurry, Qamariya Nasrullah, Travis Park and the Evans EvoMorph Lab for discussions and constructive criticism of the manuscript. Thanks to Mark Collard for supplementary information on the hominin phylogeny. We thank the Powell-Cotton Museum (Malcolm Harman) (UK), American Museum of Natural History (USA), Cleveland Museum of Natural History (USA), Royal Belgian Institute of Natural Sciences (Belgium), National Museum of Natural History (USA), The Bavarian State Collection of Zoology (Germany) for access to great ape material. For access to CT scans of fossil hominin material we thank the following individuals and institutions: National Museums of Kenya (Emma Mbua), Ditsong National Museum of Natural History (Stephany Potze), University of Witwatersrand (Colin Menter and Bernard Zipfel), Senckenberg Natural History Museum (Friedemann Schrenk and Ottmar Kullmer), and the Royal Belgian Institute of Natural Sciences (Michel Toussaint). This study made use of material from the Burlington Growth Centre, Faculty of Dentistry, University of Toronto, which was supported by funds provided by Grant (1) (No. 605-7-299) National Health Grant (Canada), (data collection); (2) Province of Ontario Grant PR 33 (duplicating) and (3) the Varsity Fund (for housing and collection). All research protocols were reviewed and granted exemption by ASU's Institutional Review Board and the Burlington Growth Centre. This research was financially supported by grants from the Australian Research Council Future Fellowship (FT130100968), Academy of Finland, National Science Foundation (GRFP No. 2011121784), Max Planck Society, Wenner-Gren Foundation (K.K.C. Dissertation Grant), Graduate and Professional Student Association at ASU, and ASU Sigma XI chapter.

Author contributions
J.J. and A.R.E. conceived the project. A.R.E., E.S.D., K.K.C., K.S.P., S.J.K., M.M.S., G.C.T., G.T.S. and J.J. collected data. E.S.D. and K.K.C. independently validated application of the inhibitory cascade model to deciduous premolars. G.T.S. performed hominin taxonomic classification. M.M.S. conducted the computed tomography scanning and measurements. J.-J.H. and G.C.T. provided materials. A.R.E. performed the analyses. H.P.N. implemented individual-level prediction accuracy calculations. A.R.E. and J.J. took the lead in writing the paper with contributions from all coauthors.

Author Information Reprints and permissions information is available at www.nature.com/reprints. The authors declare no competing financial interests. Readers are welcome to comment on the

online version of this article at www.nature.com/nature. Correspondence and requests for materials should be addressed to A.R.E. (alistair.evans@monash.edu).

Fig. 1 | All hominins show the inhibitory cascade pattern for dp3-dp4-m1 triplet, but species of *Homo* show greater reduction in size of posterior molars. a, Area (mediodistal length × buccolingual width) of each lower postcanine primary tooth for seven of the 15 hominin species in this study. The inhibitory cascade predicts a linear relationship of the sizes of three adjacent teeth, as seen for dp3-dp4-m1 triplet and dp4-m1-m2 triplet for *Paranthropus boisei*. Dotted line shows expected linear relationship for dp3-dp4-m1 triplet for *Ardipithecus ramidus* and star shows predicted size of undiscovered dp4 (73 mm^2). Mean ± S.E. of populations for *Homo sapiens* (dark blue), and of individuals for fossil hominin species. **b**, Measurements of tooth area used in this study illustrated on *Homo erectus* Sangiran 1B: mesiodistal length × buccolingual width, 3D EDJ area, 2D crown area and 2D cervix area.

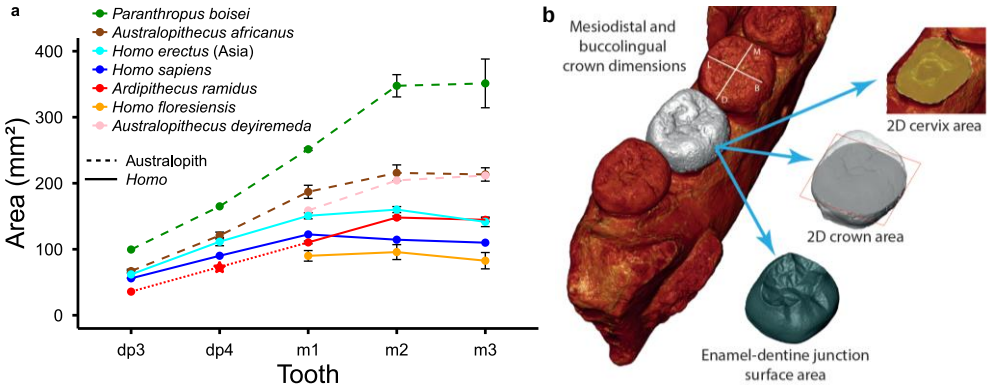

Fig. 2 | Prediction surfaces for hominin tooth sizes based on inhibitory cascade and scaling of inhibitory cascade reversal with m1 size. Tooth area (vertical axis) for each tooth position (dp3-m3) and area of m1. Tooth areas and surface for *Homo* species are plotted in blue, and australopiths in red. Vertical lines connecting spheres to surface show deviation of the species means from predicted size. See Supplementary Movie 5 for 3D rotating graph animation.

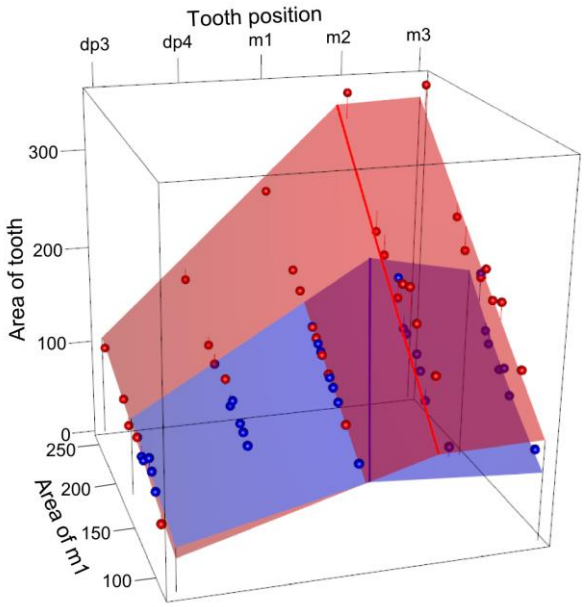

Fig. 3 | Hominin prediction plot for primary postcanine rows. a, c, Contour plot of prediction surfaces in Fig. 2. Contours show tooth areas in mm^2. Blue contours are for *Homo* species (**c**) and red for australopiths (**a**). From the mean size of one tooth position (e.g. an australopith m1 of 250 mm^2), the mean sizes of the remaining four teeth in the row can be predicted. To do so, find the known tooth's position on the x-axis and move vertically (orange arrow) to find the red contour matching the measured size. Then move horizontally (green arrows) to the other tooth positions (green crosses) to locate the predicted sizes according to the red contours. Asterisks and dashed lines indicate position of inhibitory cascade reversal, which is the position of maximum tooth size of the row. **b**, Predicted tooth row sizes for mean m1 areas of 175 and 250 mm^2 for australopiths and 125 mm^2 for *Homo*, which are similar in size to the species listed below each tooth row. Lines above tooth rows indicate triplets that follow the inhibitory cascade (deviation from inhibitory cascade less than 5%).

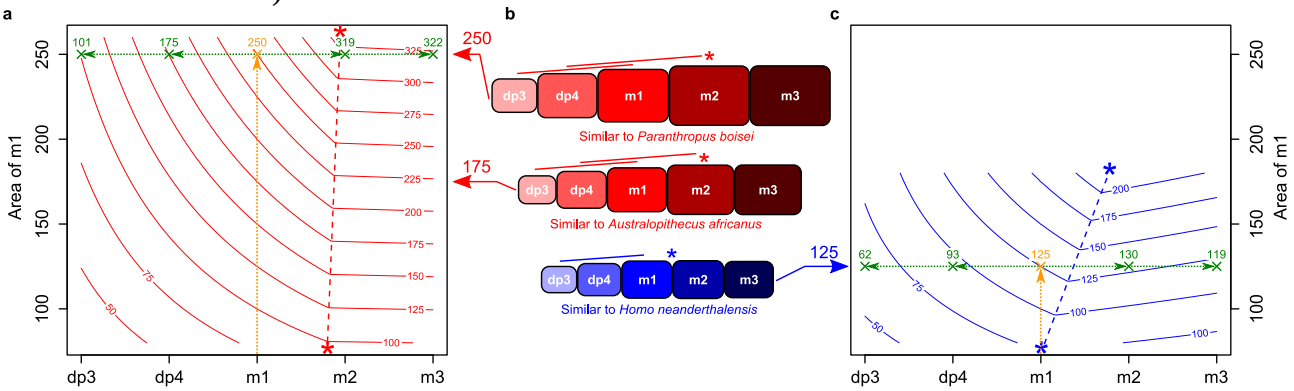

Fig. 4 | Phylogenetic distribution of tooth sizes and proportions in hominins shows an origin of the *Homo* pattern shortly after the origin of the genus. Tooth sizes plotted to scale for all species in the current study. Supplementary Spreadsheet 1 was used to predict measurements for unavailable tooth positions. The largest tooth for the species mean is filled black, as is any other tooth that is within 5% of the size of the largest tooth. The largest tooth/teeth for fossil individuals with all three molars preserved is indicated with a white circle. The phylogeny is modified from Dembo *et al.*[31] to include only taxa represented in this study, with the addition of *Pan paniscus*, *Pongo pygmaeus* and *Australopithecus deyiremeda* (***) (see Supplementary Information).

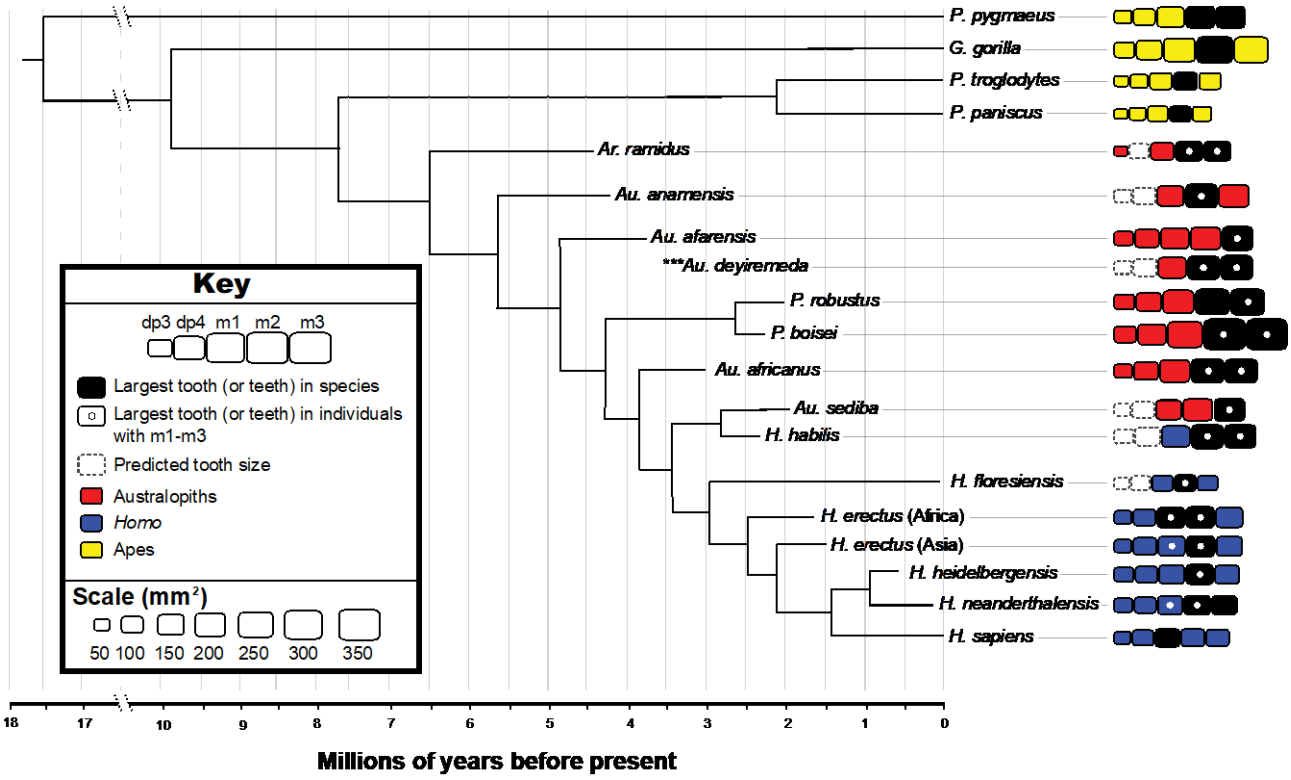

Extended Data

Evans *et al.* (2015). A simple rule governs the evolution and development of hominin tooth size.

Extended Data Fig. 1 | *Homo* species and australopiths differ in their pattern of tooth sizes, but all hominins and great apes follow the inhibitory cascade for dp3-dp4-m1 triplet. The inhibitory cascade predicts that there is a linear relationship among three adjacent teeth. Area (mm^2) of each lower postcanine primary tooth. **a**, Mean area of each tooth for 15 hominin species. **b-e**, Red points and lines are species means. **b**, *Homo sapiens*, black points and lines represent means of populations. **c**, eight australopith species and **d**, six fossil *Homo* species, black points and lines represent individual tooth rows (left and right rows of each specimen plotted separately). **e**, Four great ape species, black points and lines represent means of each sex. **f**, Two great ape species, black points and lines represent individuals, red points and lines are means for each sex. Sex and species means show clearer inhibitory cascade patterns than most individuals.

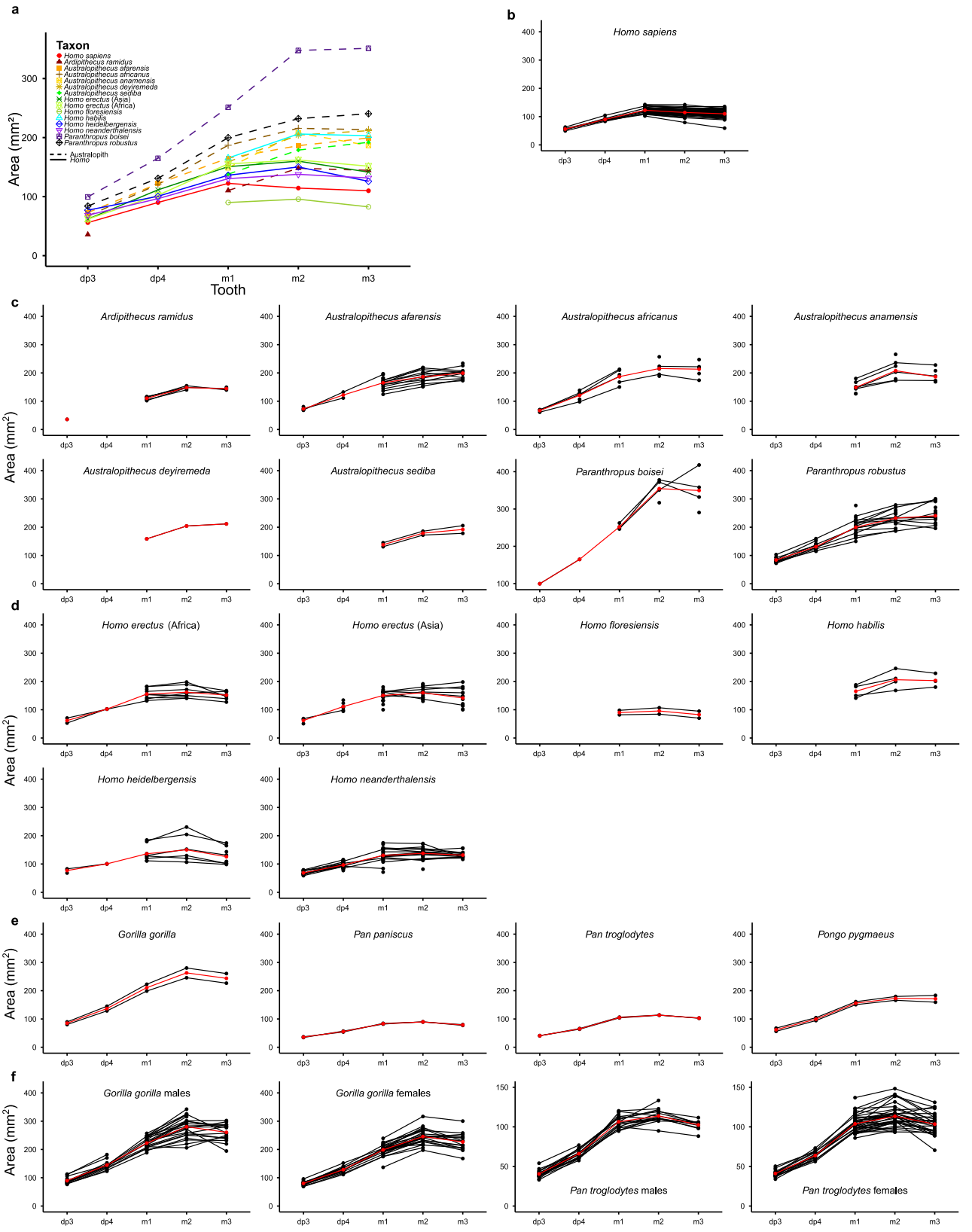
a
Taxon
Homo sapiens
Ardipithecus ramidus
Australopithecus afarensis
Australopithecus africanus
Australopithecus anamensis
Australopithecus deyiremeda
Australopithecus sediba
Homo erectus (Asia)
Homo erectus (Africa)
Homo floresiensis
Homo habilis
Homo heidelbergensis
Homo neanderthalensis
Paranthropus boisei
Paranthropus robustus
Australopith
Homo
Area (mm²)
Tooth
dp3
dp4
m1
m2
m3
b
Homo sapiens
c
Ardipithecus ramidus
Australopithecus afarensis
Australopithecus africanus
Australopithecus anamensis
Australopithecus deyiremeda
Australopithecus sediba
Paranthropus boisei
Paranthropus robustus
d
Homo erectus (Africa)
Homo erectus (Asia)
Homo floresiensis
Homo habilis
Homo heidelbergensis
Homo neanderthalensis
e
Gorilla gorilla
Pan paniscus
Pan troglodytes
Pongo pygmaeus
f
Gorilla gorilla males
Gorilla gorilla females
Pan troglodytes males
Pan troglodytes females

Extended Data Fig. 2 | The proportional size of each tooth shows a tight relationship with absolute size of the first molar, with the relationship differing between *Homo* species, australopiths and great apes. Proportional size of each tooth (proportion of the largest tooth in the row) vs area of m1 (mm^2) for 15 hominin and 4 great ape species. Blue triangles and solid line, OLS regression for *Homo* species; red circles and dashed line, OLS for australopiths; yellow squares and dotted line, OLS for great apes.

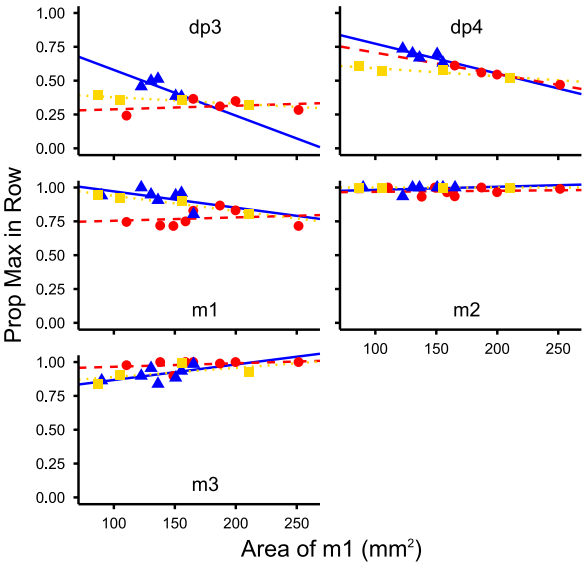

Extended Data Fig. 3 | Tooth proportions of hominins are constrained by the inhibitory cascade and size of m1. 3D space of tooth position (horizontal axis, numbered 1-5 for dp3-m3), area of m1 (axis into page) and proportion of maximum in tooth row (vertical axis). The proportional sizes of all teeth lie on two planes in 3D space. For all groups, Plane A is fit to dp3-dp4-m1, and Plane B to m2-m3. **a**, *Homo* species, Plane A (cyan; R^2 = 0.96) formula: HomoAPropMaxinRow = 0.238×ToothPos - 0.00166×AreaM1 + 0.441. Plane B (blue; R^2 = 0.62) formula: HomoBPropMaxinRow = -0.0822×ToothPos + 0.000690×AreaM1 + 1.23. Thick blue line shows intersection of planes. **b**, Australopiths, Plane A (light red; R^2 = 0.93) formula: AustAPropMaxinRow = 0.0810×ToothPos + 0.230×AreaM1 + 2.38×10^{-6}. Plane B (dark red; R^2 = 0.07) formula: AustBPropMaxinRow = 0.00963×ToothPos + 0.000168×AreaM1 + 0.906. Thick red line shows intersection of planes. **c**, Great apes, Plane A (yellow; R^2 = 0.98) formula: ApeAPropMaxinRow = 0.268×ToothPos - 0.0727×AreaM1 + 0.173. Plane B (light brown; R^2 = 0.63) formula: ApeBPropMaxinRow = -0.0837×ToothPos + 0.000337×AreaM1 + 1.29. While the R^2 values are substantially lower for the Plane B regressions, the average deviation from Plane B for *Homo* and australopiths is 0.026 and 0.022 respectively, which are lower than the compared to equivalent values of 0.046 and 0.036 for Plane A. Therefore, the low R^2 values do not reflect the close fit of the data to the planes. **d**, Comparison of *Homo*, australopith and great ape planes shows that the corresponding planes and intersections for the first two groups diverge at smaller m1 sizes. The great ape planes fall between those of the other two groups. See Supplementary Movies 1-4 for 3D rotating graph animations.

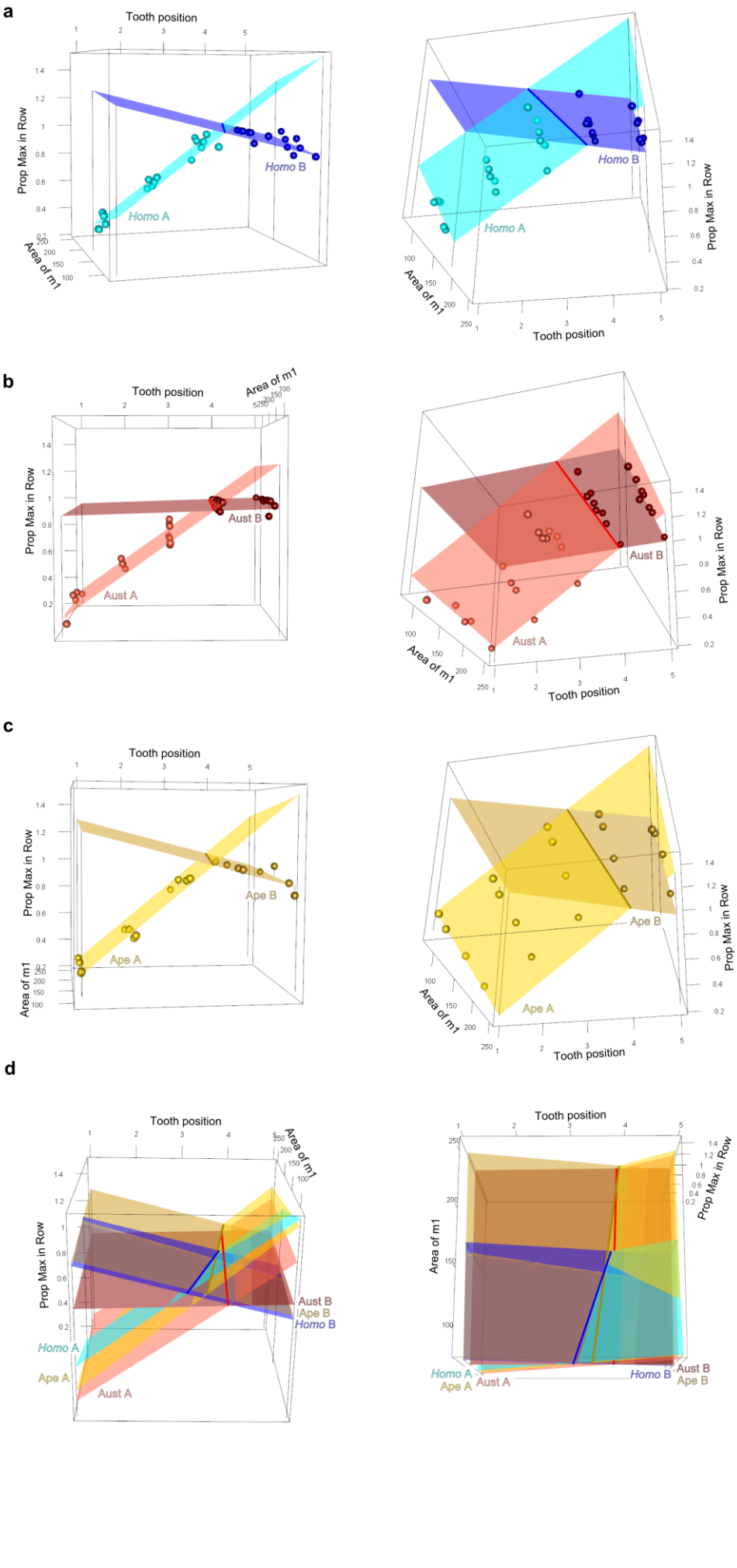
a
Tooth position
Prop Max in Row
Area of m1
Homo B
Homo A
Tooth position
Area of m1
Prop Max in Row
Homo B
Homo A
b
Tooth position
Area of m1
Prop Max in Row
Aust B
Aust A
Area of m1
Prop Max in Row
Aust B
Aust A
Tooth position
c
Tooth position
Prop Max in Row
Area of m1
Ape B
Ape A
Area of m1
Prop Max in Row
Ape B
Ape A
Tooth position
d
Tooth position
Area of m1
Prop Max in Row
Aust B
Ape B
Homo B
Homo A
Ape A
Aust A
Tooth position
Area of m1
Prop Max in Row
Homo A
Ape A
Aust A
Homo B
Aust B
Ape B

Extended Data Fig. 4 | The size of the largest tooth in the row is closely related to the size of the m1 in hominins. OLS regressions. HomoMaxAreaInRow = 1.312×AreaM1 - 30.44, p = 0.001, R^2 = 0.90; AustMaxAreaInRow = 1.298×AreaM1 + 0.150, p = 0.0003, R^2 = 0.90.

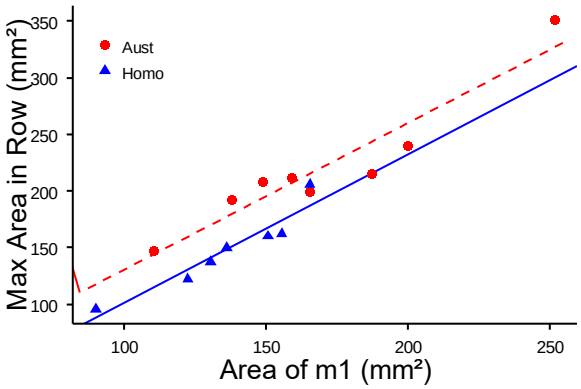

Extended Data Fig. 5 | Percentage error in estimates of each tooth compared to the prediction surfaces in Fig. 2. Prediction surface is calculated so that m1 always has zero prediction error, therefore it is excluded from error calculations. **a**, *Homo* species; **b**, australopiths.

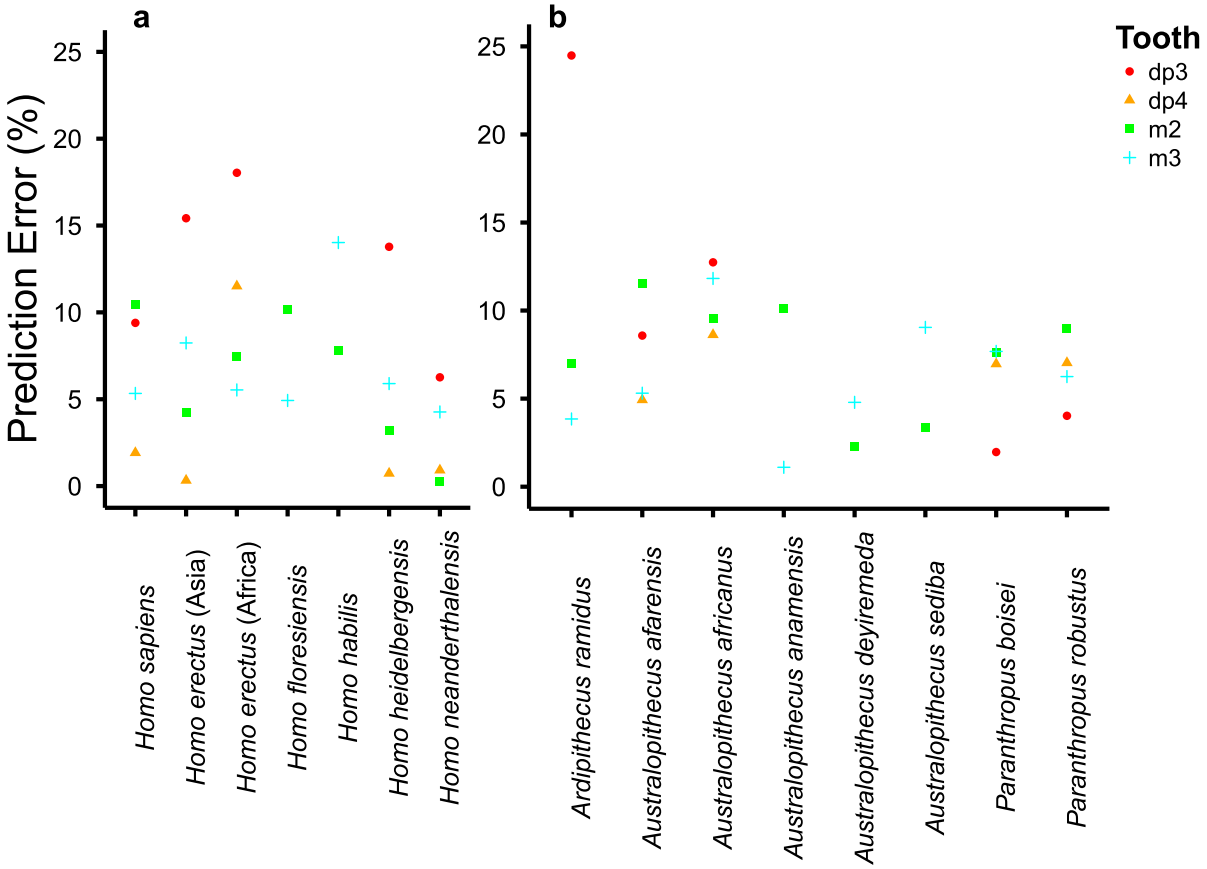

Extended Data Fig. 6 | Detailed contour plot (contour step = 5 mm^2) for prediction surfaces of hominin tooth size. Area of m1 and areas on contour in mm^2. Blue contours are for *Homo* species, red for australopiths. From the mean size of one tooth position (e.g. m1 at 125 mm^2), the mean sizes of the remaining four teeth in the row can be predicted by following the tooth position vertically (orange line) to meet the contour of the measured size, then moving horizontally to the other tooth positions (cyan line and crosses) to read off the sizes according to the contours. When mean m1 size is 125 mm^2, dp3, dp4, m2 and m3 are 62, 93, 130 and 199 mm^2 respectively for a *Homo* species and 50, 88, 156 and 158 mm^2 respectively for an australopith species.

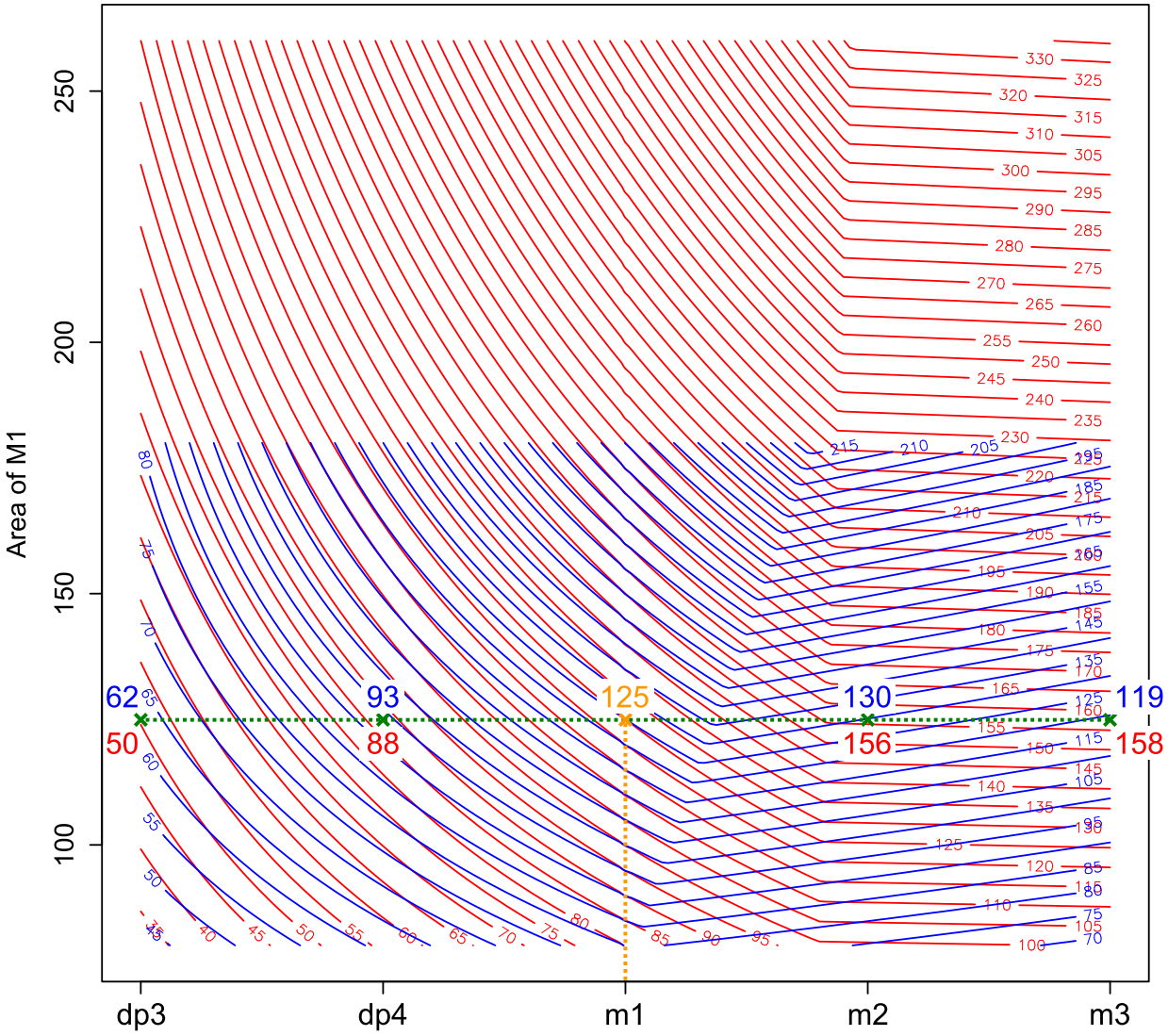

Extended Data Fig. 7 | 2D and 3D measures of tooth size for six fossil hominin specimens. Rectangular area (mesiodistal length × buccolingual width, MDBLArea), 3D area of the enamel-dentine junction (EDJ3DArea), cross-sectional area of the tooth at the cervix (CervixArea) and outline area of the outer enamel surface (OES2DArea) for each tooth position.

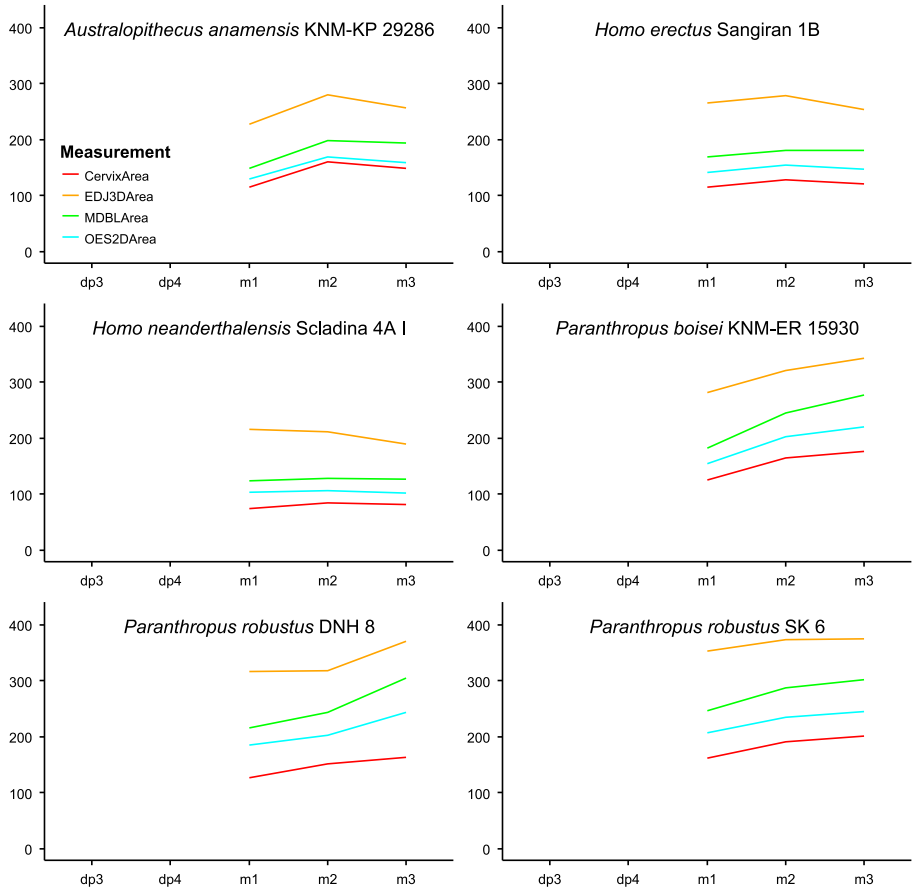

Extended Data Fig. 8 | 2D and 3D measures of tooth size are highly correlated. Bivariate plots for planar area (mesiodistal length × buccolingual width, MDBLArea), 3D area of the enamel-dentine junction (EDJ3DArea), cross-sectional area of the tooth at the cervix (CervixArea) and outline area of the outer enamel surface (OES2DArea). R^2 shown for each plot.

	CervixArea	EDJ3DArea	MDBLArea
EDJ3DArea	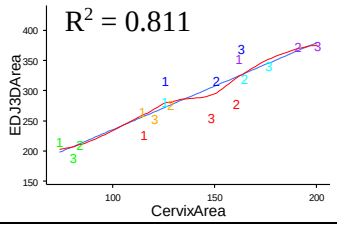		
MDBLArea	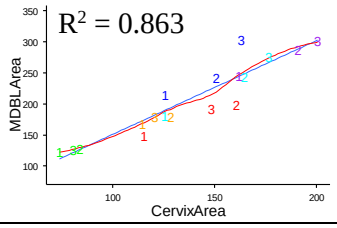	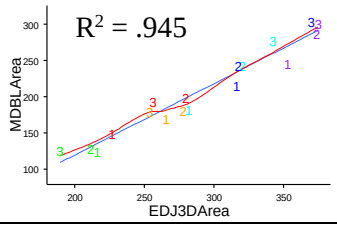	
OES2DArea	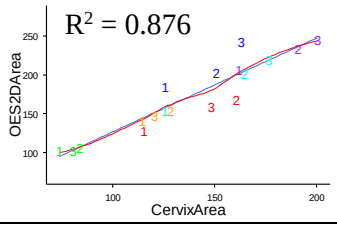	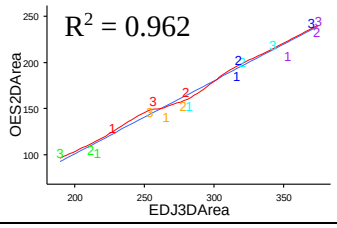	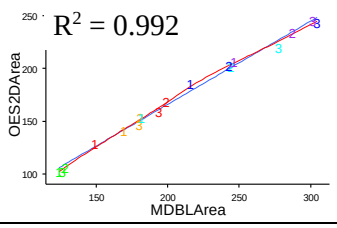

Species Specimen

- *Australopithecus anamensis* KNM-KP 29286
- *Homo erectus* Sangiran 1B
- *Homo neanderthalensis* Scladina 4A I
- *Paranthropus boisei* KNM-ER 15930
- *Paranthropus robustus* DNH 8
- *Paranthropus robustus* SK 6

Tooth

1 M1
2 M2
3 M3

Extended Data Fig. 9 | Slope of the inhibitory cascade in murines is weakly related to absolute size, unlike in hominins where there is a strong relationship. a, Relative sizes of molars for the 29 species of murine rodents in Kavanagh *et al.*[6]. **b**, Relative size of third molar to first molar (m3/m1) plotted against absolute size of first molar (mm^2) shows a weak relationship (cf. Extended Data Fig. 2).

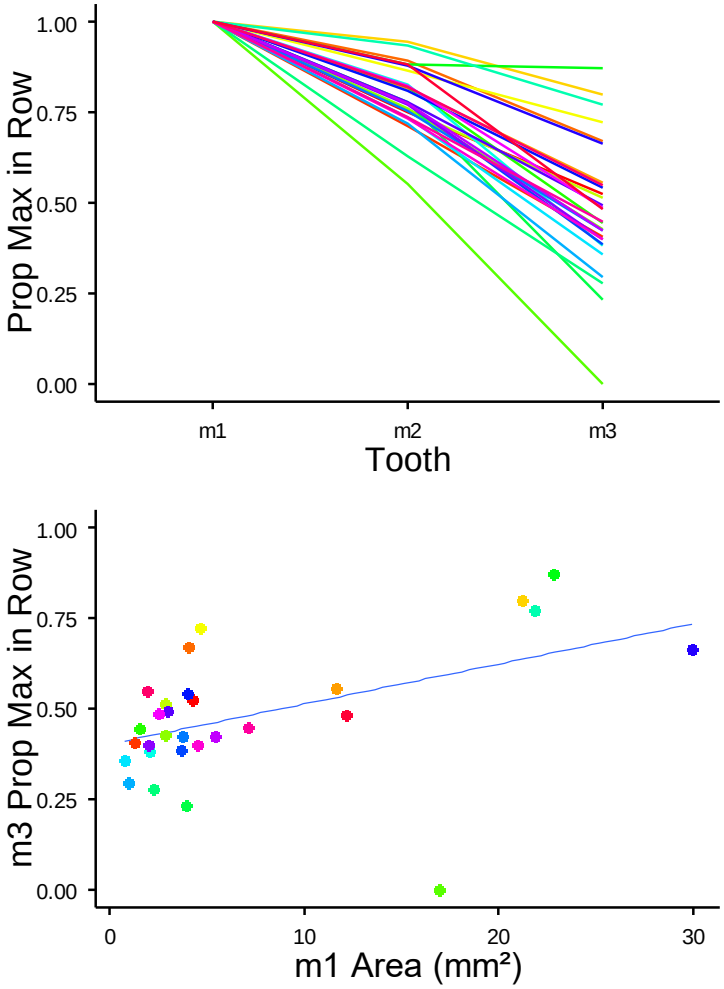

Supplementary Information

Evans *et al.* (2015). A simple rule governs the evolution and development of hominin tooth size.

Schematic diagram of results

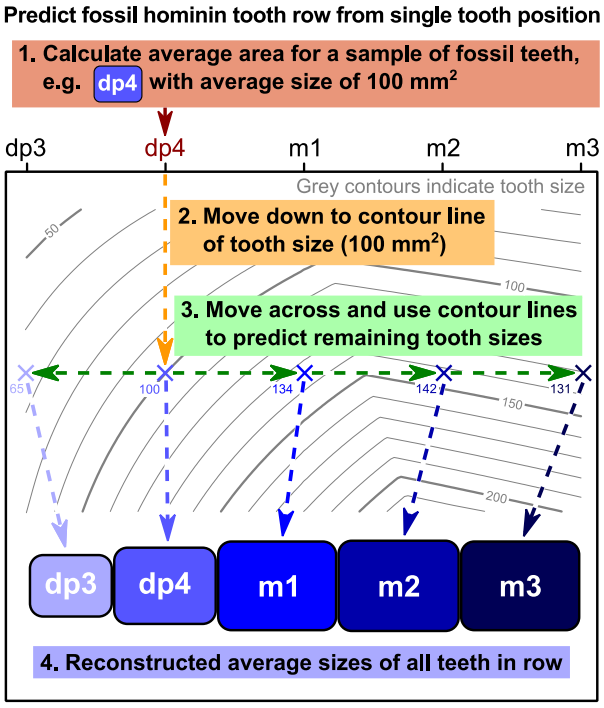

Supplementary Methods

Equivalencies of Inhibitory Cascade Pattern

The original formulation of the inhibitory cascade by Kavanagh *et al.*[6] established that the ratio of the m2/m1 varies with the ratio of the m3/m1 as:

$$\frac{m3}{m1} = 2 \times \left(\frac{m2}{m1}\right) - 1$$

Kavanagh *et al.*[6:430] showed that this is mathematically equivalent to m2 being 1/3 of the total area of the row. In addition, it can be shown that m2 is the average of m1 and m3 when the inhibitory cascade pattern is being followed:

$$\frac{m3}{m1} = 2 \times \left(\frac{m2}{m1}\right) - 1$$

$$2 \times \left(\frac{m2}{m1}\right) = \frac{m3}{m1} + 1$$

$$2 \times m2 = m1\left(\frac{m3}{m1} + 1\right)$$

$$m2 = (m1 + m3)/2$$

Therefore, m2 is the sum of m1 and m3 divided by 2, which is the average of m1 and m3.

We can also show that the pattern is linear when the inhibitory cascade is being followed, i.e. that the change from m1 to m2 (given by $m2 - m1$) is the same as from m2 to m3 (given by $m3 - m2$):

$$m2 = (m1 + m3)/2$$

$$2 \times m2 = m1 + m3$$

$$m2 - m1 = m3 - m2$$

Therefore, these four statements are mathematically equivalent, and all express the expected pattern according to the inhibitory cascade:

1. m3/m1 = 2×(m2/m1) – 1
2. m2 is 1/3 of the total of the tooth row.
3. m2 is the average of m1 and m3.
4. The change in sizes across three teeth, m1, m2 and m3, is linear.

All of these statements are true whether the absolute tooth size is used (e.g. in mm^2) or if they are some proportion (e.g. percentage of largest tooth in the row, or percentage of m1).

Derivation of Prediction Surface

Variables:

PropArea, area of tooth as a percentage of largest tooth in the row. $PropAreaA$ and $PropAreaB$ represent proportional area of tooth for regions A and B respectively.

T, tooth position (1 to 5 for dp3 to m3)

$AM1$, area of first molar (m1), tooth position 3

Ta, tooth position slope coefficient for *PropArea*

Aa, area of m1 slope coefficient for *PropArea*

Pb, intercept coefficient for *PropArea*

MaxArea, absolute area of largest tooth in the row

Ma, slope coefficient for *MaxArea*

Mb, intercept coefficient for *MaxArea*

Area, area of teeth for given tooth position and area of m1. $AreaA$ and $AreaB$ represent proportional area of tooth for regions A and B respectively.

$AreaAStA$ area of teeth in region A for given tooth position and area of m1, standardized by $AreaA$ at m1.

$AreaBStA$ area of teeth in region B for given tooth position and area of m1, standardized by $AreaA$ at m1.

We use the planar regressions that describe the proportional size of each tooth for each tooth position and the size of the m1 in that row.

General regression equation for multiple linear regression of $PropArea$ vs T and $AM1$:

$$PropArea = Ta \times T + Aa \times AM1 + Pb \quad \text{Eq. 1}$$

The hominin tooth size data are divided into two regions, A and B, where Region A is where tooth positions are 1, 2 and 3, while Region B is where tooth positions are 4 and 5.

OLS regression equations for Plane A (data in Region A) calculated from *Homo* data based on Eq. 1:

$$PropAreaAH = 0.2378 \times T + -0.001658 \times AM1 + 0.4406 \quad \text{Eq. 2}$$

OLS regression equations for Plane B (data in Region B) calculated from *Homo* data based on Eq. 1:

$$PropAreaBH = -0.08217 \times T + 0.0006890 \times AM1 + 1.226 \quad \text{Eq. 3}$$

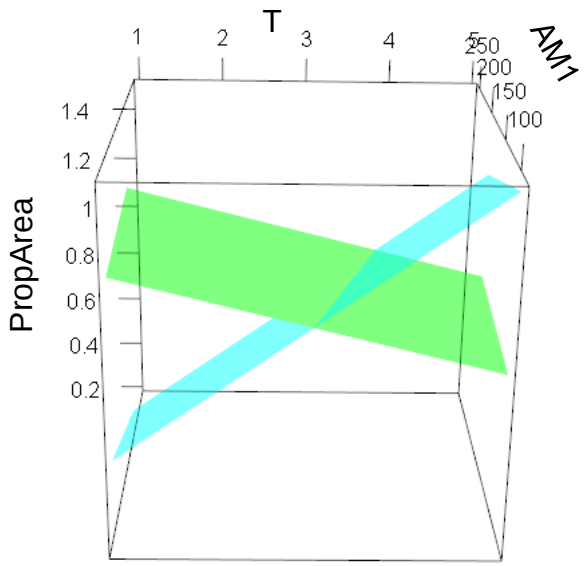

Fig. S1 | Plot of tooth position *T* (horizontal) vs area of m1 *AM1* (into page) vs proportion of area *PropArea* (vertical). Plane A (cyan) and Plane B (green). The two regions that represent the data are Plane A on the left of the intersection and Plane B on the right of the intersection of the two planes.

The tooth position at which the maximum tooth size occurs is the 'reversal' position, which is the intersection between Planes A and B. The intersection between Planes A and B can be found by setting Eq. 2 equal to Eq. 3:

$$PropAreaA = PropAreaB \quad \text{Eq. 4}$$

$$0.2378 \times T + -0.001658 \times AM1 + 0.4406 = -0.08217 \times T + 0.0006890 \times AM1 + 1.226 \quad \text{Eq. 5}$$

Solve Eq. 5 for $AM1$:

$$AM1H = -426.1(0.7852 - 0.3199 \times T) \quad \text{Eq. 6}$$

$MaxArea$ gives the expected size of the largest tooth for a given m1 size:

$$MaxArea = Ma \times AM1 + Mb \quad \text{Eq. 7}$$

Regression equation for *Homo* data based on Eq. 7 (see Extended Data Fig. 4):

$$MaxAreaH = 1.312 \times AM1 - 30.44 \quad \text{Eq. 8}$$

The area of each tooth in a row (mm^2) can be estimated by multiplying the proportional size of each tooth in the row ($PropArea$) by the expected maximum area for the size of m1 in that row ($MaxArea$).

$$Area = PropArea \times MaxArea \quad \text{Eq. 9}$$

$$= (Ta \times T + Aa \times AM1 + Pb) \times (Ma \times AM1 + Mb) \quad \text{Eq. 10}$$

Formula for $AreaAH$ for *Homo* (substituting equation for Plane A (Eq. 2) and Eq. 8 into Eq. 10):

$$AreaAH = (0.2378 \times T + -0.001658 \times AM1 + 0.4406) \times (1.312 \times AM1 - 30.44) \quad \text{Eq. 11}$$

Formula for $AreaBH$ for *Homo* (substituting equation for Plane B (Eq. 3) and Eq. 8 into Eq. 10):

$$AreaBH = (-0.08217 \times T + 0.0006890 \times AM1 + 1.226) \times (1.312 \times AM1 - 30.44) \quad \text{Eq. 12}$$

The resulting surfaces show how the areas of all teeth in the row can be calculated given the tooth position (T) and the area of the m1 ($AM1$) in that row (Fig. S2).

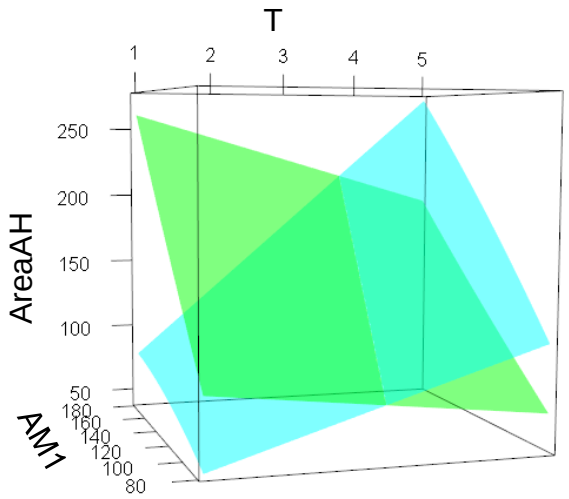

Fig. S2 | Plot of *T* (horizontal) vs *AM1* (into page) vs *Area* (vertical). *AreaAH* is cyan surface and *AreaBH* is green surface. The two regions that represent the data are *AreaAH* on the left of the intersection and *AreaBH* on the right of the intersection.

The expected relationship between predicted m1 size and actual m1 size is linear, where slope = 1. However, when the *Area* formulas are used to predict m1 size, the relationship between predicted m1 area and actual m1 area is not linear because the cross-section through the surface (i.e. *AreaAH*) at $T = 3$ (i.e. at m1) is not a linear function with slope = 1 and intercept = 0. For example, if the *Area* formula is used to predict the area of m1 ($AM1$), given $Area = 80$ and $T = 3$, then the predicted area of m1 is $AM1 \approx 76.1$, not the expected value of 80. The non-linear relationship is illustrated in Fig. S3, which is a cross-section of the cyan surface in Fig. S2 at $T = 3$. The expected 1:1 relationship is shown in black, while *AreaAH* diverges from the 1:1 relationship.

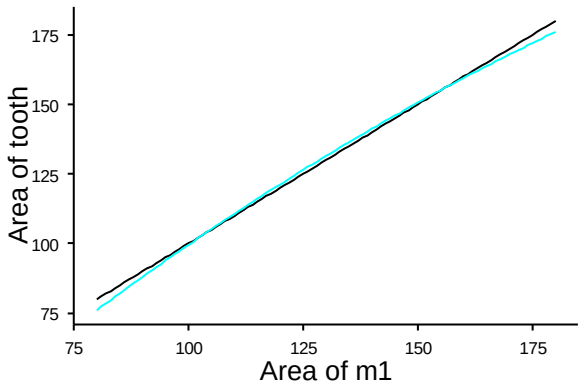

Fig. S3 | Prediction of m1 area using formulas for *AreaAH* (cyan) when $T = 3$ compared to the expected 1:1 relationship (black). If the cyan formula were standardized by the expected value (black), the standardized cyan surface will correctly predict m1 size.

To ensure that the cross-section at $T = 3$ is always 1:1, *Area* can be standardized by dividing by the ratio of calculated m1 area ($AM1$ when $T = 3$; Eq. 13) to m1 area (Eq. 14). This forces the

prediction surface at m1 to be a 1:1 linear function of *AM1*, so m1 size is always predicted correctly. The standardized area is *AreaSt*.

$$AreaAtM1 = (Ta \times 3 + Aa \times AM1 + Pb) \times (Ma \times AM1 + Mb) \quad \text{Eq. 13}$$

$$AreaSt = \frac{Area}{\left(\frac{AreaAtM1}{AM1}\right)} \quad \text{Eq. 14}$$

$$= \frac{(Ta \times T + Aa \times AM1 + Pb) \times (Ma \times AM1 + Mb)}{\left(\frac{(Ta \times 3 + Aa \times AM1 + Pb) \times (Ma \times AM1 + Mb)}{AM1}\right)} \quad \text{Eq. 15}$$

Substituting Eq. 11 and Eq. 13 into Eq. 15 gives *AreaAH* standardized by the value of m1 on *AreaAH*:

$$AreaAHStA = \frac{AreaAH}{\left(\frac{AreaAHAtM1}{AM1}\right)} \quad \text{Eq. 16}$$

$$AreaAHStA = \frac{(0.2378 \times T + -0.001658 \times AM1 + 0.4406) \times (1.312 \times AM1 - 30.44)}{\left(\frac{(0.2378 \times T + -0.001658 \times 3 + 0.4406) \times (1.312 \times AM1 - 30.44)}{AM1}\right)} \quad \text{Eq. 17}$$

AreaB standardized by the value of m1 on *AreaA* is:

$$AreaBHStA \frac{AreaBH}{\left(\frac{AreaAHAtM1}{AM1}\right)} \quad \text{Eq. 18}$$

$$AreaBHStA = \frac{(-0.08217 \times T + 0.0006890 \times AM1 + 1.226) \times (1.312 \times AM1 - 30.44)}{\left(\frac{(0.2378 \times T + -0.001658 \times 3 + 0.4406) \times (1.312 \times AM1 - 30.44)}{AM1}\right)} \quad \text{Eq. 19}$$

To calculate the predicted sizes for a given tooth position and size, the *Area* formulas were solved for *AM1* using Wolfram Mathematica 8.0, taking the quadratic solution that corresponds with the tooth area data.

$$AM1AreaAHStA = 4.011 \times 10^{-29} \times \left(3.313 \times 10^{30} + 1.247 \times 10^{28} AreaAH - \sqrt{(-4.327 \times 10^{59} AreaAH + (-3.313 \times 10^{30} - 1.247 \times 10^{28} AreaAH - 1.788 \times 10^{30} T)^2)} + 1.788 \times 10^{30} T\right) \quad \text{Eq. 20}$$

$$AM1AreaBHStA = 8.380 \times 10^{-24} \times \left(-1.062 \times 10^{26} - 1.436 \times 10^{23} AreaBH + 7.116 \times 10^{24} T + \sqrt{(2.385 \times 10^{49} AreaBH + (-1.062 \times 10^{26} - 1.436 \times 10^{23} AreaBH + 7.116 \times 10^{24} T)^2)}\right) \quad \text{Eq. 21}$$

Eq. 20 and Eq. 21 are used in Supplementary Spreadsheet 1 to predict the size of the m1 in the row of Tooth X (the mean size of a sample of teeth of a given position). From the predicted size of the m1, the sizes of the remainder of the teeth in the row are predicted in Supplementary Spreadsheet 1 using Eq. 17 and Eq. 19 given the region of each tooth on the prediction surface.

OLS regression equations for Plane A (data in Region A) calculated from australopith data based on Eq. 1:

$$PropAreaAA = 0.2304 \times T + 2.379 \times 10^{-6} \times AM1 + 0.08096$$ Eq. 22

OLS regression equations for Plane B (data in Region B) calculated from australopith data based on Eq. 1:

$$PropAreaBA = 0.009631 \times T + 0.0001680 \times AM1 + 0.9062$$ Eq. 23

$$AM1A = -6037(0.8253 - 0.2208 \times T)$$ Eq. 24

Max area for australopiths:

$$MaxAreaA = 1.298 \times AM1 + 0.1495$$ Eq. 25

Following the same steps as above using the australopith data give the following prediction equations:

$$\begin{aligned} AM1AreaAAStA = {} & 1.973 \times 10^{-12} \\ & \times \left(-8.625 \times 10^{15} + 2.534 \times 10^{11} AreaAA \right. \\ & + \sqrt{(8.341 \times 10^{28} AreaAA + (-8.625 \times 10^{15} + 2.534 \times 10^{11} AreaAA - 2.455 \times 10^{16} T)^2)} - 2.455 \\ & \left. \times 10^{16} T \right) \end{aligned}$$ Eq. 26

$$\begin{aligned} AM1AreaBAStA = {} & 5.587 \times 10^{-17} \\ & \times \left(-4.827 \times 10^{19} + 1.267 \times 10^{14} AreaBA \right. \\ & + \sqrt{(1.473 \times 10^{26} AreaBA + (-4.827 \times 10^{19} + 1.267 \times 10^{14} AreaBA - 5.130 \times 10^{17} T)^2)} - 5.130 \\ & \left. \times 10^{17} T \right) \end{aligned}$$ Eq. 27

Calculation of Confidence Intervals for Predictions in Supplementary Spreadsheet 1

The calculation of the 95% confidence intervals cannot be done using the usual approach[32] since the predicted means are estimated as the product of two independent distributions. The regression of the maximum tooth size is done using the model matrix (X_m), a new point (x_m) at which a prediction is made, a standard error (s_m) and the regression coefficients (β_m), and yields the distribution of the prediction (m)

$$\frac{m - \beta_m x_m}{s_m \sqrt{x_m^T (X_m^T X_m)^{-1} x_m}} \sim t(df_m).$$

The two relative size planes are regressed using a model matrix (X_p), the standard error (s_p), and regression coefficients (β_p). Once the appropriate plane is determined, the prediction (p) is distributed

$$\frac{p - \beta_p x_p}{s_p \sqrt{x_p^T (X_p^T X_p)^{-1} x_p}} \sim t(df_p).$$

A derivation of the formulas is available[32]. The product distribution of the product of these two estimates can be calculated, but has no closed form solution. As such, a numerical approach is used. For each new point, *mp* is estimated by taking a random sample of 100,000 student t variables on the appropriate number of degrees of freedom and the t variables are substituted in each equation above, and the product *mp* is taken. The 2.5th quantile and the 97.5th quantile are then taken from this resulting sample from the product distribution.

This approach works for any new point at which a model prediction is made. However, to

implement this in Excel, a simplification was made to ease computational complexity. A cubic spline was fit to each of the tooth positions at intervals of 1 mm^2 in m1 size, on the range of existing m1 sizes.

Phylogenetic Tree

The phylogeny in Fig. 4 is modified from Dembo *et al.*[31] to include only taxa represented in this study. The divergence date for *P. pygmaeus* was set at 17.5 mya[33] and the split between *P. paniscus* and *P. troglodytes* at 2.1 mya[34]. The placement of *A. deyiremeda* (***) is based on the date of 3.3-3.5 mya and the phylogenetic position suggested in Haile-Selassie *et al.*[17].

Supplementary Information

Evans *et al.* 2015. A simple rule governs the evolution and development of hominin tooth size.

Tables

Supplementary Table 1 | *Homo sapiens* population-level mean rectangular area (mesiodistal length × maximum buccolingual width, mm^2) of lower deciduous premolars and molars. These studies have data for both deciduous premolar and at least two molars from the same population, sometimes published in separate references. Sex: B, both; F, female; M, male.

Population	Sex	dp3	dp4	m1	m2	m3	Source
Icelanders	F			118.41	108.21		[35]
Icelanders	M			125.03	116.14		[35]
Icelanders	F	56.74	89.77				[36]
Icelanders	M	58.66	91.87				[36]
Chicago Whites	B	55.15	86.90				[37]
Chicago Whites	M			116.06	113.19	104.35	[37]
Jats (Haryana, India)	F	52.74	86.39	107.50	94.47		[38]
Jats (Haryana, India)	M	55.76	90.44	112.96	102.11		[38]
Yuendumu Aborigines	F	60.66	101.42				[39]
Yuendumu Aborigines	M	65.19	107.27				[39]
Yuendumu Aborigines	F			132.86	124.54	127.43	[40]
Yuendumu Aborigines	M			142.29	132.03	135.99	[40]
Michigan Whites	F	56.51	84.75	103.31	89.97		[41]
Michigan Whites	M	57.95	87.91	112.03	99.50		[41]
Burlington Growth Centre, Toronto	F	48.41	81.54	108.56	98.68		[42]
Burlington Growth Centre, Toronto	M	50.73	84.79	115.59	106.29		[42]
Late Archaic/Glacial Kame	B	54.27	93.60				[43]
Late Archaic/Glacial Kame	B			126.55	118.55	107.70	[44]
South Australian caucasoid	F	59.35	85.90	117.70	113.73		[45]
South Australian caucasoid	M	57.62	88.98	123.34	117.06		[45]

Supplementary Table 2 | *Homo sapiens* population-level mean rectangular area (mesiodistal length × buccolingual width, mm^2) of lower molars. Sex: B, both; F, female; M, male. Comp: Compilation source.

Region	Population	Sex	m1	m2	m3	Source	Comp.
Africa	American Negros	B	128.52	130.80	129.60	[46]	[23]
Africa	Negro (S. Africa)	F	118.22	112.45	111.53	[47]	[28]
Africa	Negro (S. Africa)	M	123.70	119.00	116.70	[47]	[28]
Africa	Negro (W. Africa, Teso)	B	119.45	112.72	126.28	[48]	[28]
Africa	Nubian Agriculturalist (3300-1100BC)	F	113.18	104.53	98.30	[49]	[28]
Africa	Nubian Agriculturalist (3300-1100BC)	M	124.25	116.30	109.50	[49]	[28]
Africa	Nubian Intensive Agriculturalist (1-1400AD)	F	109.65	102.89	93.98	[49]	[28]
Africa	Nubian Intensive Agriculturalist (1-1400AD)	M	120.26	112.33	105.26	[49]	[28]
Africa	Nubian Mesolithic (10000-7000BC)	F	125.10	118.81	113.83	[49]	[28]
Africa	Nubian Mesolithic (10000-7000BC)	M	139.24	130.19	124.88	[49]	[28]
Africa	San (Bushman, Kalahari nomadic)	F	111.37	110.09	95.65	[50]	[28]
Africa	San (Bushman, Kalahari nomadic)	M	114.14	110.77	102.11	[50]	[28]
Africa	San (Bushman, skeletal)	B	111.18	107.06	95.04	[51]	[28]
Africa	San (Bushman, skeletal)	F	117.72	106.05	90.24	[52]	[28]
Africa	San (Bushman, skeletal)	M	94.50	110.21	101.00	[52]	[28]
Africa	San (Bushmen, Kalahari settlers)	F	111.62	107.32	98.01	[50]	[28]
Africa	San (Bushmen, Kalahari settlers)	M	101.57	114.49	99.50	[50]	[28]
Africa	Wadi Halfa Mesolithic	B	139.15	135.70	135.70	[53]	[23]
Asia	Chinese	M	120.89	111.27	109.71	[54] in [47]	[28]
Asia	Chinese (Bronze Age Shang Dynasty)	B	120.33	112.35	108.64	[55]	[28]
Asia	Chinese (Hong Kong)	B	113.42	106.28	99.77	[55]	[28]
Asia	India (Bronze Age Harappans)	F	106.58	91.57	83.06	[56]	[28]
Asia	India (Bronze Age Harappans)	M	111.41	100.28	94.02	[56]	[28]
Asia	India (Inagaon 1700-700BC)	B	123.56	107.95	109.44	[57]	[28]
Asia	India (Ramapuram)	M	114.13	101.88	104.75	[58]	[28]
Asia	IndiaPunjabi	B	115.19	105.03	104.48	[59]	
Asia	Indonesians (Gilimanuk)	B	127.60	118.77	113.36	[60]	[23]
Asia	Japanese (Ainu Hokkaido)	F	111.28	97.00	89.24	[61]	[28]
Asia	Japanese (Ainu Hokkaido)	M	122.10	106.05	97.92	[61]	[28]
Asia	Japanese (Early Jomon)	F	120.99	105.04	98.94	[61]	[28]
Asia	Japanese (Early Jomon)	M	128.82	113.40	107.06	[61]	[28]
Asia	Japanese (Early Yayoi)	F	124.30	111.28	108.12	[61]	[28]
Asia	Japanese (Early Yayoi)	M	135.70	125.40	114.40	[61]	[28]
Asia	Japanese (Hokoriku)	F	116.63	108.12	91.20	[62] in [47]	[28]
Asia	Japanese (Hokoriku)	M	120.96	115.50	102.00	[62] in [47]	[28]
Asia	Japanese (Korean descent)	F	117.70	111.28	96.03	[61]	[28]
Asia	Japanese (Korean descent)	M	127.68	122.04	114.40	[61]	[28]
Asia	Japanese (Kyoto)	F	117.66	113.36	97.92	[61]	[28]

Region	Population	Sex	m1	m2	m3	Source	Comp.
Asia	Japanese (Kyoto)	M	127.65	120.91	106.05	61	28
Asia	Japanese (Tokyo, Edo Period)	F	118.77	113.36	103.95	61	28
Asia	Japanese (Tokyo, Edo Period)	M	126.50	119.78	108.07	61	28
Asia	Malay	B	125.06	115.28	106.30		23
Asia	South-east (Bronze Age Java)	B	127.20	121.03	117.71	55	28
Asia	South-east (Bronze Age Thai)	B	125.85	112.25	105.74	55	28
Asia	South-east (Java)	B	125.93	110.96	104.71	55	28
Asia	South-east (Java)	F	119.84	106.08	109.14	63	28
Asia	South-east (Java)	M	126.50	114.45	113.36	63	28
Asia	South-east (Thai)	B	123.48	112.85	113.82	55	28
Asia	Tibet	F	100.86	78.86	62.07	64	28
Asia	Tibet	M	103.50	79.94	56.40	64	28
Australia	Broadbeach	F		133.28	117.52	65	28
Australia	Broadbeach	M	142.68	151.04	139.15	65	28
Australia	Western Australia	F	119.74	126.00	119.46	66	28
Australia	Western Australia	M	139.32	136.89	133.02	66	28
Australia	Yuendumu	F	132.93	124.98	126.33	67,68	28
Australia	Yuendumu	M	142.67	132.82	132.47	67,68	28
Europe	American Whites	B	126.14	110.09	114.13		23
Europe	Caucasoid	B	120.40	115.11	111.57		23
Europe	Lapps (Skolt)	F	116.95	109.30	104.03	69	28
Europe	Lapps (Skolt)	M	123.18	115.23	108.04	69	28
Europe	Norwegian Lapps	F	111.72	96.78	88.04	22	28
Europe	Norwegian Lapps	M	113.88	105.84	94.25	22	28
North America	Dickson Mound	B	130.13	124.65	119.77	23	23
North America	Eskimo (Hall Beach)	M	131.04	122.21		70	28
North America	Eskimo (Igloolik)	F	120.99	115.56	114.49	70	28
North America	Eskimo (Igloolik)	M	132.21	126.56	128.80	70	28
North America	Eskimo, Aleut	F	115.25	121.87	117.75	71	28
North America	Eskimo, Aleut	M	122.07	118.39	112.97	71	28
North America	Indian Knoll (4160-2558BC)	F	125.96	117.16	117.07	72	28
North America	Indian Knoll (4160-2558BC)	M	133.80	123.40	120.27	72	28
North America	Ohio Valley (Adena)	F	120.58	113.14	103.94	44	28
North America	Ohio Valley (Adena)	M	124.17	119.01	108.37	44	28
North America	Ohio Valley (Hopewell)	F	120.73	112.47	111.57	44	28
North America	Ohio Valley (Hopewell)	M	132.28	124.12	119.72	44	28
North America	Pecos Pueblo (800-1100AD)	B	128.45	119.46	112.41	73	28
North America	Tennessee Archaic (6000-500BC)	B	119.77	115.67	114.17	74	28
North America	Tennessee Mississippi (1300-1550AD)	B	120.59	114.02	107.20	74	28
North America	Tennessee Woodland (700-1150AD)	B	124.65	119.23	118.26	74	28
Oceania	Bougainville (Nasioi)	F	122.49	112.78	106.49	75	28
Oceania	Bougainville (Nasioi)	M	130.74	122.10	115.53	75	28
Oceania	New Britain	B	133.48	123.52	125.91	76	23
Oceania	New Britain (West Nakanai)	M	120.75	105.00	113.30	77	28
Oceania	New Guinea (Goroka)	M	139.95	130.98	125.18	78	28

Region	Population	Sex	m1	m2	m3	Source	Comp.
Oceania	New Guinea (Lufa)	M	139.88	130.04	120.19	[78]	[28]
South America	Lengua	F	125.53	110.58	104.54	[79]	[28]
South America	Lengua	M	132.26	119.65	115.85	[79]	[28]
South America	Peruvian (2500-1000BP)	B	122.04	114.48	104.04	[80]	[28]
South America	Peruvian (4000-2500BP)	B	115.56	111.28	112.35	[80]	[28]
South America	Peruvian (6500-4000BP)	B	117.66	111.24	99.96	[80]	[28]

Supplementary Table 3 | Fossil hominin specimen-level rectangular area (mesiodistal length × buccolingual width, mm^2) of lower deciduous premolars and molars. Side: L, left; R, right; U, unknown.

Species	Specimens	Side	dp3	dp4	m1	m2	m3	Source
Ardipithecus ramidus	ARA-VP-1/128	L			111.1	154.7		[81]
Ardipithecus ramidus	ARA-VP-1/128	R			115.36		139.7	[81]
Ardipithecus ramidus	ARA-VP-1/129	R	35.77					[81]
Ardipithecus ramidus	ARA-VP-1/200	L			113.3			[81]
Ardipithecus ramidus	GWM16/P10	R					149.345	[82]
Ardipithecus ramidus	GWM3/P1	R			102	147.32		[82]
Ardipithecus ramidus	GWM3W/P185	L			107.625			[82]
Ardipithecus ramidus	GWM5SW/P56	L			118.8	148.59		[82]
Ardipithecus ramidus	GWM5SW/P56	R			113.42	148.59	144.64	[82]
Ardipithecus ramidus	GWM9N/P50	L			102.82	140.12		[82]
Ardipithecus ramidus	GWM9N/P50	R			107			[82]
Ardipithecus ramidus	KNM-TH 13150	R			115.44	149.34		[83]
Australopithecus afarensis	AL 128-23	L			124.32	151.25		[84]
Australopithecus afarensis	AL 145-35	L			174.2	218.68		[84]
Australopithecus afarensis	AL 188-1	R					234.08	[84]
Australopithecus afarensis	AL 198-1	L				153.76	176.66	[84]
Australopithecus afarensis	AL 200-1b	R			162.5			[84]
Australopithecus afarensis	AL 207-13	L				165		[84]
Australopithecus afarensis	AL 241-14	L			197.1			[84]
Australopithecus afarensis	AL 266-1	L			149.94			[84]
Australopithecus afarensis	AL 266-1	R			152.32	182	207	[84]
Australopithecus afarensis	AL 277-1	L				218.95		[84]
Australopithecus afarensis	AL 288-1i	L					173.24	[84]
Australopithecus afarensis	AL 288-1i	R			136.4	161.04	172.02	[84]
Australopithecus afarensis	AL 333-30	R	68					[84]
Australopithecus afarensis	AL 333-43	L	75.05	109.98				[84]
Australopithecus afarensis	AL 333-43	R	72.38	112.52				[84]
Australopithecus afarensis	AL 333-74	L			182.25		195.96	[84]
Australopithecus afarensis	AL 333w-1	L			159.72	168.75		[84]
Australopithecus afarensis	AL 333w-1	R			158.6	180.7		[84]
Australopithecus afarensis	AL 333w-12	R			166.37			[84]
Australopithecus afarensis	AL 333w-27	L				217.14		[84]
Australopithecus afarensis	AL 333w-32,60	L			174.24	211.7	204.48	[84]
Australopithecus afarensis	AL 333w-32,60	R					200.22	[84]
Australopithecus afarensis	AL 333w-48	R				152.46		[84]
Australopithecus afarensis	AL 333w-57	L				173.03	180	[84]
Australopithecus afarensis	AL 333w-59	L				201.6	183.4	[84]
Australopithecus afarensis	AL 400-1a	L			161.2	221.92	202.5	[84]
Australopithecus afarensis	AL 400-1a	R			168.91	213.15	212.52	[84]
Australopithecus afarensis	AL 417-1d	L			143.84	170.3	198.17	[85]
Australopithecus afarensis	LH 2	L		131.44				[86]
Australopithecus afarensis	LH 2	R	69.16	133.56	194.6			[86]
Australopithecus afarensis	LH 3	R	80.64		180.88			[86]
Australopithecus afarensis	LH 4	L				201.28		[86]
Australopithecus afarensis	LH 4	R			167.58		225.78	[86]
Australopithecus afarensis	MAK-VP-1/12	L			159.82	186.2	205.02	[87]
Australopithecus afarensis	MAK-VP-1/12	R			157.3	188.86	203.68	[87]
Australopithecus afarensis	MAK-VP-1/2	R			168.64	195	202.8	[87]

Species	Specimens	Side	dp3	dp4	m1	m2	m3	Source
Australopithecus africanus	MLD 2	U		138.43	212.8			88,89
Australopithecus africanus	MLD 5	R		125.66				89
Australopithecus africanus	Sts 18	R		123.6	209.89			90
Australopithecus africanus	Sts 24	L	62.05					91
Australopithecus africanus	Sts 24	R	60.48	98.1	150.29			89
Australopithecus africanus	Sts 4	U				188.76		90
Australopithecus africanus	Sts 41	U					197.81	90
Australopithecus africanus	Sts 52b	L				196.84	173.99	90
Australopithecus africanus	Sts 52b	R			167.7	192.96	174.15	90
Australopithecus africanus	Sts 6	U				214.2		90
Australopithecus africanus	Sts 7	L				223.38	221.76	90
Australopithecus africanus	Sts 9	U			193.7			90
Australopithecus africanus	Stw 106	L	69.92	129.54				89
Australopithecus africanus	Stw 123	L		106.7				89
Australopithecus africanus	Taung	L		124.02	185.9			88,89
Australopithecus africanus	Taung	R	69.6	123.05	189			90
Australopithecus africanus	TM 1515	U				257.04		90
Australopithecus africanus	TM 1518	U					247.16	90
Australopithecus africanus	TM 1519	U					218.23	90
Australopithecus africanus	TM 1520	U					220.8	90
Australopithecus anamensis	ARI-VP-1/352	R					170.17	92
Australopithecus anamensis	ARI-VP-3/176	R				265.68		92
Australopithecus anamensis	ARI-VP-3/80	R				178.92		92
Australopithecus anamensis	KNM-ER 20422	L			126.44			93
Australopithecus anamensis	KNM-ER 20428	L					207.7	93
Australopithecus anamensis	KNM-KP 29286	L			146.37		188.76	94
Australopithecus anamensis	KNM-KP 29286	R			145.14	203	188.94	94
Australopithecus anamensis	KNM-KP 30500	L			179.55	238.58		94
Australopithecus anamensis	KNM-KP 30500	R			180.78	233.73	227.8	94
Australopithecus anamensis	KNM-KP 34725	L	63.92		167.14	224		95
Australopithecus anamensis	KNM-KP 29281	L			151.13	172.62	175.68	94
Australopithecus anamensis	KNM-KP 29281	R			151.2	175.14	170.17	94
Australopithecus anamensis	KNM-KP 31712	L		83.43	127.05			95
Australopithecus anamensis	KNM-KP 31717	L					169.88	95
Australopithecus anamensis	KNM-KP 31729	R		82.45				95
Australopithecus anamensis	MSD-VP-3/24	L					168.74	92
Australopithecus anamensis	MSD-VP-5/16	L			143.99	173.24		92
Australopithecus deyiremeda	BRT-VP-3/14	R			158.76	204.24	211.72	17
Australopithecus sediba	MH1	R			145	185.76	205.62	96
Australopithecus sediba	MH2	R			130.98	172.02	180.34	96
Australopithecus sediba	MH2	L					176.25	96
Homo erectus (Asia)	D 211	L			162.5	133.4	113.42	97
Homo erectus (Asia)	D 211	R			162.36	141.45	118.72	97
Homo erectus (Asia)	D 2600	L				180.7	187.5	98
Homo erectus (Asia)	D 2600	R				186.26	208.81	98
Homo erectus (Asia)	D 2735	L			147.84	138.6		98
Homo erectus (Asia)	D 2735	R			154.28	145.52		98
Homo erectus (Asia)	Hexian PA 831	U					120.91	99
Homo erectus (Asia)	Hexian PA 834	U			163.75	180.88		99
Homo erectus (Asia)	Hexian PA 838	U				189.04		99
Homo erectus (Asia)	Hexian PA 839	U				191.62		99

Species	Specimens	Side	dp3	dp4	m1	m2	m3	Source
Homo erectus (Asia)	Lantian	R			144.9	163.8		[99]
Homo erectus (Asia)	PCG2	L		107.67				[100]
Homo erectus (Asia)	Sangiran 9	R				179.07	175.26	[101] in [97]
Homo erectus (Asia)	Sangiran 1B	U			162.5	171.6	181.25	[102]
Homo erectus (Asia)	Sangiran FS67	R	66.24					[103]
Homo erectus (Asia)	Sangiran FS72	R		134				[103]
Homo erectus (Asia)	Zhoukoudian G1-6	L			165	158.75	147.6	[104] in [97]
Homo erectus (Asia)	Zhoukoudian G1-7	R				162.54	159.96	[104] in [97]
Homo erectus (Asia)	ZKD 100	L			165			[104]
Homo erectus (Asia)	ZKD 101	U			118.65			[104]
Homo erectus (Asia)	ZKD 102	L			163.8			[104]
Homo erectus (Asia)	ZKD 106	U				135.66		[104]
Homo erectus (Asia)	ZKD 110	U				158.75		[104]
Homo erectus (Asia)	ZKD 111	U				158.76		[104]
Homo erectus (Asia)	ZKD 114	U					100	[104]
Homo erectus (Asia)	ZKD 115	U					159.96	[104]
Homo erectus (Asia)	ZKD 116	U					147.6	[104]
Homo erectus (Asia)	ZKD 117	U					102	[104]
Homo erectus (Asia)	ZKD 123	U	50.82					[104]
Homo erectus (Asia)	ZKD 125, ZKD 128	R	68.6	98.28				[104]
Homo erectus (Asia)	ZKD 126	U		94.5				[104]
Homo erectus (Asia)	ZKD 127	R		123.22				[104]
Homo erectus (Asia)	ZKD 129	R		110.88				[104]
Homo erectus (Asia)	ZKD 131	U					137.16	[104]
Homo erectus (Asia)	ZKD 134	U					113.42	[104]
Homo erectus (Asia)	ZKD 136	U					117.72	[104]
Homo erectus (Asia)	ZKD 137	U			152.1			[104]
Homo erectus (Asia)	ZKD 138	U				129.95		[104]
Homo erectus (Asia)	ZKD 147	U			143.91			[104]
Homo erectus (Asia)	ZKD 34	U			132.98			[104]
Homo erectus (Asia)	ZKD 35	R			157.5			[104]
Homo erectus (Asia)	ZKD 36	L			180.48			[104]
Homo erectus (Asia)	ZKD 38	L			99.99			[104]
Homo erectus (Asia)	ZKD 43	U				142.08		[104]
Homo erectus (Asia)	ZKD 44	U				150.65		[104]
Homo erectus (Asia)	ZKD 45	U				145.2		[104]
Homo erectus (Asia)	ZKD 51	U					147.62	[104]
Homo erectus (Asia)	ZKD 52	U					139.08	[104]
Homo erectus (Asia)	ZKD 96	R			132.16			[104]
Homo erectus (Asia)	ZKD 97	R			132.09			[104]
Homo erectus (Asia)	ZKD 98	R			171.36			[104]
Homo erectus (Asia)	ZKD 99	R			163.48			[104]
Homo erectus (Africa)	KNM-ER 1507	L	53.04	102.83				[89]
Homo erectus (Africa)	KNM-ER 1808	R					163.2	[105]
Homo erectus (Africa)	KNM-ER 820	L	71.1	100.58	131.61			[106]
Homo erectus (Africa)	KNM-ER 820	R	70.07	103.4	131.76			[106]
Homo erectus (Africa)	KNM-ER 992	L			138.43	158.6	164.82	[101] in [97]
Homo erectus (Africa)	KNM-WT 15000	L			132.98	140.3		[107]
Homo erectus (Africa)	KNM-WT 15000	R			132.09	141.36		[107]
Homo erectus (Africa)	OH 22	R			153.4	147.32		[108]
Homo erectus (Africa)	OH 51	L			172.62			[108]

Species	Specimens	Side	dp3	dp4	m1	m2	m3	Source
Homo erectus (Africa)	Ternifine I	R			165	171.6	152.5	[109] in [110]
Homo erectus (Africa)	Ternifine II	L			182	189	167.5	[109] in [110]
Homo erectus (Africa)	Ternifine III	R			153.75	150.06	139.2	[109] in [110]
Homo erectus (Africa)	Thomas I	L			182	198	146.37	[111] in [110]
Homo erectus (Africa)	Rabat	U			143	141.25	127.2	[102]
Homo floresiensis	LB1	R			98.04	107	95	[112]
Homo floresiensis	LB6-1	U			82	84.39	70.31	[112]
Homo habilis	OH 13	L			150.8		180.56	[113]
Homo habilis	OH 13	R			149.64	168.19	179.58	[113]
Homo habilis	OH 16	R			187.96	246.13	228.8	[113]
Homo habilis	OH 27	R					201.96	[113]
Homo habilis	OH 37	L			141.24	199.5		[113]
Homo habilis	OH 4	R					201.5	[113]
Homo habilis	OH 7	L			180.56	210.6		[113]
Homo habilis	OH 7	R			183.52			[113]
Homo heidelbergensis	Arago 1	L		100.7				[89]
Homo heidelbergensis	Arago 1	R	82.82					[89]
Homo heidelbergensis	Arago 13	U			184.96	204.4	174.2	[97]
Homo heidelbergensis	Arago 2	U			119.9	129.71	101.85	[110]
Homo heidelbergensis	Arago 22	R	68.25					[89]
Homo heidelbergensis	Arago 5	L		100.44				[89]
Homo heidelbergensis	Arago 6	R	80					[114] in [115]
Homo heidelbergensis	Arago 8	R			179.4	230.74	165	[110]
Homo heidelbergensis	AT 1	L			125.4	117.42	96.6	[110]
Homo heidelbergensis	AT 1	R			131.08	123.12	107.91	[110]
Homo heidelbergensis	AT 100	L					109	[110]
Homo heidelbergensis	AT 101	R			111.24			[110]
Homo heidelbergensis	AT 11	L				107		[110]
Homo heidelbergensis	AT 13	L					143.51	[110]
Homo heidelbergensis	AT 2	R			124.02			[110]
Homo heidelbergensis	AT 21	L			136.8			[110]
Homo heidelbergensis	AT 22, AT 75	L			111.28	106.92	98.44	[110]
Homo heidelbergensis	AT 30	R					107.67	[110]
Homo heidelbergensis	Mauer	L					129.95	[102]
Homo heidelbergensis	Mauer	R			129.92	152.4	132.98	[102]
Homo neanderthalensis	Amud 1	L			117.72	113.4	127.44	[116]
Homo neanderthalensis	Amud 1	R			118.8	116.39	121.8	[116]
Homo neanderthalensis	Amud III	R		95.68				[116]
Homo neanderthalensis	Archi	L	66.6	95.68				[117] in [115]
Homo neanderthalensis	Archi	R	69.3	98.58				[117] in [115]
Homo neanderthalensis	Barakai	U		111.1				[118] in [119]
Homo neanderthalensis	Couvin	R		87				[119]
Homo neanderthalensis	Cova Negra	R		87.87				[120]
Homo neanderthalensis	Dederiyeh 1	L	66.3	102.6	120.75			[121]
Homo neanderthalensis	Dederiyeh 1	R	68.8					[121]
Homo neanderthalensis	Dederiyeh 2	L	64.38	94.94				[122]
Homo neanderthalensis	Engis 2	R	58.8	90.9				[123] in [115]
Homo neanderthalensis	Fate 12	L				126.44		[124]
Homo neanderthalensis	Fate 2	L			113			[124]
Homo neanderthalensis	Fate 3	R					139.7	[124]
Homo neanderthalensis	Fate 5	L		85.85				[124]
Homo neanderthalensis	Fate 6	R			138.75			[124]

Species	Specimens	Side	dp3	dp4	m1	m2	m3	Source
Homo neanderthalensis	Gibralter 2	L	72.54	108.78				[125,126]
Homo neanderthalensis	Gibralter 2	R	76.56	105.06				[125,127]
Homo neanderthalensis	Grotte du Bison I Q5.1	R		81.7				[128]
Homo neanderthalensis	Grotte du Bison I S6	R		87				[128]
Homo neanderthalensis	Grotte du Renne 16	R				81.84		[129]
Homo neanderthalensis	Grotte du Renne 18	R	72.96					[129]
Homo neanderthalensis	Grotte du Renne 21	R				146.16		[129]
Homo neanderthalensis	Grotte du Renne 25	R	63					[129]
Homo neanderthalensis	Grotte du Renne 29	R		89				[129]
Homo neanderthalensis	Grotte du Renne 30	R			71.44			[129]
Homo neanderthalensis	Grotte du Renne 33	R	60.59					[129]
Homo neanderthalensis	Grotte du Renne 35	R			133.2			[129]
Homo neanderthalensis	Grotte du Renne 5	R				141.52		[129]
Homo neanderthalensis	Grotte du Renne 6	R					122.04	[129]
Homo neanderthalensis	Hortus 15	L		83.72				[130] in [115]
Homo neanderthalensis	Hortus 2	L		83.72				[130] in [125]
Homo neanderthalensis	KMH 1	L	65.52	92.92	84.15			[131]
Homo neanderthalensis	KMH 1	R	67.5	91.35				[131]
Homo neanderthalensis	KMH 14	L				140		[131]
Homo neanderthalensis	KMH 2	L				117.72	118.77	[131]
Homo neanderthalensis	KMH 2	R				120.99	123.17	[131]
Homo neanderthalensis	KMH 32	U				127.6		[131]
Homo neanderthalensis	Krapina 1, Krapina 7, Krapina 79	R			174.795	172.36	122.5	[132]
Homo neanderthalensis	Krapina 10, Krapina 77, Krapina 108	R			154.24	154.945	140.065	[132]
Homo neanderthalensis	Krapina 104	R			112.32			[132]
Homo neanderthalensis	Krapina 105	R			170			[132]
Homo neanderthalensis	Krapina 107	L				170.8		[132]
Homo neanderthalensis	Krapina 2, Krapina 84	R			125.97	141.45		[132]
Homo neanderthalensis	Krapina 3, Krapina 5, Krapina 82	L			154.2	142.945	140.79	[132]
Homo neanderthalensis	Krapina 4	L					128.26	[132]
Homo neanderthalensis	Krapina 51	L	77.9					[132]
Homo neanderthalensis	Krapina 52, Krapina 62	L		85.2025	116.28			[132]
Homo neanderthalensis	Krapina 53	R		109.545	151.875	160.475		[132]
Homo neanderthalensis	Krapina 54, Krapina 83	L			123.585	112.7		[132]
Homo neanderthalensis	Krapina 55, Krapina 106	L			157.3	150.93	136.53	[132]
Homo neanderthalensis	Krapina 57	R			143.125	143.22	129.34	[132]
Homo neanderthalensis	Krapina 58	L			127.53	135.09	128.4	[132]
Homo neanderthalensis	Krapina 58	R			129.6	136.23	132.37	[132]
Homo neanderthalensis	Krapina 59	L			130.98	140.3		[132]
Homo neanderthalensis	Krapina 59	R					133.34	[132]
Homo neanderthalensis	Krapina 6	L				135.85		[132]
Homo neanderthalensis	Krapina 63	L		115.575				[132]
Homo neanderthalensis	Krapina 64	L	77.42	91.91	130.68			[132]
Homo neanderthalensis	Krapina 65	L		102.46				[132]
Homo neanderthalensis	Krapina 66	L		106.5				[132]

Species	Specimens	Side	dp3	dp4	m1	m2	m3	Source
Homo neanderthalensis	Krapina 68	R		112.86				[132]
Homo neanderthalensis	Krapina 78	L					116.48	[132]
Homo neanderthalensis	Krapina 8	R					155.68	[132]
Homo neanderthalensis	Krapina 80	R			146.05			[132]
Homo neanderthalensis	Krapina 85	L					126.42	[132]
Homo neanderthalensis	Krapina 86	L				145.41		[132]
Homo neanderthalensis	Krapina 9	L					125.19	[132]
Homo neanderthalensis	La Ferrassie 4 *bis*	L		76.8				[133] in [115]
Homo neanderthalensis	La Ferrassie 8	L	62.16	101.37				[133] in [115]
Homo neanderthalensis	La Ferrassie 8	R	62.25					[133] in [115]
Homo neanderthalensis	La Quina 761	R		99.75				[134] in [119]
Homo neanderthalensis	Molare	L		118.65				[115]
Homo neanderthalensis	Molare	R	79.2	110.74				[115]
Homo neanderthalensis	Pech de lAze	R	65.25	92.92				[125]
Homo neanderthalensis	Roc de Marsal infant	L	66	96.46				[135]
Homo neanderthalensis	Roc de Marsal infant	R	65.7	99.64				[135]
Homo neanderthalensis	Salemas	L		110				[136] in [135]
Homo neanderthalensis	Scladina 4A-13	R		89.3				[119]
Homo neanderthalensis	Shanidar 1	L			105	117.72	124.2	[137]
Homo neanderthalensis	Shanidar 1	R			109.2	121	126.44	[137]
Homo neanderthalensis	Shanidar 2	L			126.44	135.6	131.04	[137]
Homo neanderthalensis	Shanidar 2	R			124.32	129.92	120.96	[137]
Homo neanderthalensis	Shanidar 6	R				148.68	156.16	[137]
Homo neanderthalensis	Shanidar 7	L	67.64	91				[138]
Homo neanderthalensis	Shanidar 7	R	61.92					[138]
Homo neanderthalensis	Tabun series IV	L		105.28				[139:209] in [119]
Homo neanderthalensis	Teshik-Tash	L	78.3	96.9				[140] in [125]
Homo neanderthalensis	Teshik-Tash	R	76.5	105.6				[140] in [125]
Paranthropus boisei	KNM-ER 1477	L	97.9	168.51				[141]
Paranthropus boisei	KNM-ER 1477	R	101.2	161.46				[141]
Paranthropus boisei	KNM-ER 3230	L			262.4	372.13	332.1	[105]
Paranthropus boisei	KNM-ER 3230	R			246.33	377.88	358.28	[105]
Paranthropus boisei	KNM-ER 729	R			248	351	418	[142]
Paranthropus boisei	OH 26	R					290.5	[113]
Paranthropus boisei	OH 30	L			252			[113]
Paranthropus boisei	OH 38	R				316.8		[113]
Paranthropus robustus	DNH 10	R					230.79	[143]
Paranthropus robustus	DNH 18	R					270.04	[143]
Paranthropus robustus	DNH 19	L				252.32		[143]
Paranthropus robustus	DNH 2	L		117.16				[143]
Paranthropus robustus	DNH 21	L				212.67	195.91	[143]
Paranthropus robustus	DNH 44	R	94.16					[143]
Paranthropus robustus	DNH 46	R			198.45			[143]
Paranthropus robustus	DNH 51	R				233.52	236.3	[143]
Paranthropus robustus	DNH 56	L		113.85				[143]
Paranthropus robustus	DNH 56	R		116				[143]
Paranthropus robustus	DNH 60	R	72.38	123.22	161.84	188.5		[143]
Paranthropus robustus	DNH 67	R			178.12			[143]
Paranthropus robustus	DNH 7	L			168.84	180.9	206.72	[144]
Paranthropus robustus	DNH 7	R				191.7	206.36	[144]

Species	Specimens	Side	dp3	dp4	m1	m2	m3	Source
Paranthropus robustus	DNH 75	R					231.82	[143]
Paranthropus robustus	DNH 8	L			227.65	238.5	309.42	[144]
Paranthropus robustus	DNH 8	R			223.44	229.4	291.4	[144]
Paranthropus robustus	KB 5223	L	74.26	128.75	179.8			[88]
Paranthropus robustus	KB 5223	R		128.75	178.75			[88]
Paranthropus robustus	SK 1	U				260.1		[90]
Paranthropus robustus	SK 104	U			205.5			[90]
Paranthropus robustus	SK 12	U					246.24	[90]
Paranthropus robustus	SK 1586	L				207		[145]
Paranthropus robustus	SK 1586	R				223.5	250.5	[145]
Paranthropus robustus	SK 1587	L			189.63			[145]
Paranthropus robustus	SK 1587	R				196.08		[145]
Paranthropus robustus	SK 1588	L			172.2			[145]
Paranthropus robustus	SK 1648	R					227.65	[145]
Paranthropus robustus	SK 23	L			217.56	224.96	208	[90]
Paranthropus robustus	SK 23	R			214.62	222	249.12	[90]
Paranthropus robustus	SK 25	L			205.72			[90]
Paranthropus robustus	SK 25	R			203	250.5		[90]
Paranthropus robustus	SK 34	U			208.8	270.54	297	[90]
Paranthropus robustus	SK 37	U				246.5		[90]
Paranthropus robustus	SK 3974	R			199.66			[145]
Paranthropus robustus	SK 3976	L			276.8			[145]
Paranthropus robustus	SK 3978	L	79.56	136.5				[145]
Paranthropus robustus	SK 3978	R	81.18	138.03				[145]
Paranthropus robustus	SK 438	L		141.7				[89]
Paranthropus robustus	SK 5	U				213		[90]
Paranthropus robustus	SK 55b	L		138.99	195.91			[90]
Paranthropus robustus	SK 55b	R			197.28	224.51	212.35	[90]
Paranthropus robustus	SK 6	L			243.2	275.31	292.3	[90]
Paranthropus robustus	SK 6	R			235.06	281.88	289.6	[90]
Paranthropus robustus	SK 61	L	100.7	158.27				[90]
Paranthropus robustus	SK 61	R	105.45	160.8	224.84			[90]
Paranthropus robustus	SK 62	L	85.05	143.88				[90]
Paranthropus robustus	SK 62	R		160.8				[90]
Paranthropus robustus	SK 63	L	72.54	127.2	199.8			[90]
Paranthropus robustus	SK 63	R	84.6	127.2	201.15			[90]
Paranthropus robustus	SK 64	R	92.22	134.62				[90]
Paranthropus robustus	SK 81	U					251.37	[90]
Paranthropus robustus	SK 828	U			223.08			[90]
Paranthropus robustus	SK 838	U			182			[90]
Paranthropus robustus	SK 839, SK 852	R	81					[89]
Paranthropus robustus	SK 840	U					206.4	[90]
Paranthropus robustus	SK 841	U		116.4			210.98	[90]
Paranthropus robustus	SK 842	U		125.24				[90]
Paranthropus robustus	SK 843	U			197.1	219.62		[90]
Paranthropus robustus	SK 844	U					215.28	[90]
Paranthropus robustus	SK 845	R			217.5	233.6		[90]
Paranthropus robustus	SK 846	U			200.1			[90]
Paranthropus robustus	SKW 4767	U			233.28			[146]
Paranthropus robustus	SKW 5	L				231.84		[147]
Paranthropus robustus	SKW 5	R			179.52	233.28	233.8	[147]
Paranthropus robustus	SKX 4446	U			221.65	270.18		[148]

Species	Specimens	Side	dp3	dp4	m1	m2	m3	Source
Paranthropus robustus	SKX 4446	U			221.65	270.18		[146]
Paranthropus robustus	SKX 5002	L					247.42	[149]
Paranthropus robustus	SKX 5013	U			163.2			[148]
Paranthropus robustus	SKX 5013	U			163.2			[146]
Paranthropus robustus	SKX 5014	U					258	[148]
Paranthropus robustus	SKX 5023	U			180.48			[148]
Paranthropus robustus	SKX 5023	U			180.48			[146]
Paranthropus robustus	TM 1536	L	79.38					[89]
Paranthropus robustus	TM 1536	R	76.8	116.62	149.86			[88,89]
Paranthropus robustus	TM 1601	R	85					[89]

Supplementary Table 4 | Hominin mean rectangular area (mesiodistal length × buccolingual width, mm^2) of lower deciduous premolars and molars, and number of individuals sampled at each tooth position for fossil hominin species in parentheses.

Species	dp3	dp4	m1	m2	m3
Homo sapiens	55.96	90.11	122.46	114.45	109.95
Ardipithecus ramidus	35.77 (1)	(0)	110.37 (7)	148.01 (5)	144.56 (3)
Australopithecus afarensis	72.88 (4)	121.88 (2)	165.11 (17)	186.28 (18)	199.28 (13)
Australopithecus africanus	66.93 (3)	120.80 (7)	186.97 (6)	215.66 (5)	213.31 (6)
Australopithecus anamensis	(0)	(0)	148.82 (7)	207.84 (7)	186.58 (7)
Australopithecus deyiremeda	(0)	(0)	158.76 (1)	204.24 (1)	211.72 (1)
Australopithecus sediba	(0)	(0)	137.99 (2)	178.89 (2)	191.96 (2)
Homo erectus (Asia)	61.89 (3)	111.43 (6)	150.69 (19)	160.07 (18)	141.49 (16)
Homo erectus (Africa)	61.81 (2)	102.41 (2)	155.44 (10)	162.08 (8)	151.54 (7)
Homo floresiensis	(0)	(0)	90.02 (2)	95.70 (2)	82.66 (2)
Homo habilis	(0)	(0)	165.37 (4)	206.11 (4)	203.08 (4)
Homo heidelbergensis	77.02 (3)	100.57 (2)	136.20 (9)	150.21 (7)	125.93 (9)
Homo neanderthalensis	68.61 (17)	96.52 (34)	130.50 (24)	137.74 (24)	131.57 (19)
Paranthropus boisei	99.55 (1)	164.99 (1)	251.46 (3)	347.60 (3)	351.23 (3)
Paranthropus robustus	84.02 (11)	131.00 (14)	199.79 (29)	232.09 (20)	240.40 (21)

Supplementary Table 5 | Mean, maximum and standard deviation of prediction error rates (%) for *Homo* and australopith fossil individuals. The observed size of the tooth in the 'Predicted using' column was used to predict the sizes of each other tooth in the fossil. The average prediction errors for all tooth positions and specimens were 10.3% and 7.9% for *Homo* and australopith specimens respectively. * indicates values that include *Homo neanderthalensis* KMH 1 where m1 is incompletely developed and so does not fit predictions.

Mean Error

Taxon	Predicted using	Predicted tooth				
		dp3	**dp4**	**m1**	**m2**	**m3**
Homo						
	dp3		12.0	30.1*		
	dp4	8.6		12.7*	1.8	
	m1	17.1*	9.4*		10.2	15.5
	m2		1.2	7.0		8.7
	m3			10.1	8.5	
Australopiths						
	dp3		7.8	10.0	20.0	
	dp4	7.1		6.6	14.5	9.6
	m1	9.2	7.0		8.1	7.9
	m2	16.3	12.3	7.5		7.4
	m3		7.9	7.5	7.8	

Maximum Error

Taxon	Predicted using	Predicted tooth				
		dp3	**dp4**	**m1**	**m2**	**m3**
Homo						
	dp3		36.7	62.2*		
	dp4	26.7		46.0*	1.8	
	m1	32.8*	30.1*		34.8	54.5
	m2		1.2	21.1		29.2
	m3			26.9	22.5	
Australopiths						
	dp3		19.1	29.1	20	
	dp4	16.1		16.1	17.4	19.2
	m1	22.6	19.2		22.8	23.5
	m2	16.3	14.5	18.0		21.4
	m3		15.7	29.2	27.2	

SD Error

Taxon	Predicted using	Predicted tooth				
		dp3	**dp4**	**m1**	**m2**	**m3**
Homo						
	dp3		10.9	22.8*		
	dp4	7.4		16.9*		
	m1	11.1*	10.7*		7.2	12.2
	m2			4.7		7.6
	m3			6.4	6.7	
Australopiths						
	dp3		6.0	8.5		
	dp4	5.1		4.7	4.1	13.5
	m1	6.7	5.3		5.9	7.0
	m2		3.1	4.9		5.0
	m3		11.0	6.7	5.8	

Supplementary Table 6 | Great ape mean rectangular area (mesiodistal length × buccolingual width, mm^2) of lower deciduous premolars and molars. Number of individuals is in parentheses. Sex: F, female; M, male.

Species	Sex	dp3	dp4	m1	m2	m3	Source
Gorilla gorilla	F	80.24 (20)	128.55 (16)	198.74 (35)	245.75 (28)	226.61 (17)	[150]
Gorilla gorilla	M	89.53 (16)	144.83 (13)	222.63 (30)	280.18 (23)	260.68 (17)	[150]
Pan paniscus	F	36.00 (2)	55.08 (2)	86.24 (40)	92.82 (25)	78.26 (13)	[29]
Pan paniscus	M	36.00 (3)	55.89 (4)	87.22 (33)	90.16 (17)	75.60 (12)	[29]
Pan troglodytes	F	41.09 (17)	63.8 (16)	103.79 (48)	113.35 (36)	103.44 (32)	[150]
Pan troglodytes	M	40.53 (19)	66.1 (18)	106.37 (30)	113.76 (17)	102.43 (10)	[150]
Pongo pygmaeus	F	56.32 (5)	94.28 (5)	150.56 (5)	166.06 (3)	159.29 (3)	[151]
Pongo pygmaeus	M	67.6 (9)	104.49 (9)	161.17 (12)	179.54 (6)	183.37 (3)	[151]

Supplementary Table 7 | 2D and 3D measures of tooth size for six fossil hominin specimens. Rectangular area (mesiodistal length × maximum buccolingual width, MDBLArea), 3D area of the enamel-dentine junction (EDJ3DArea), cross-sectional area of the tooth at the cervix (CervixArea) and outline area of the outer enamel surface (OES2DArea) for each tooth position.

Species	Specimen	Tooth	Cervix Area	EDJ3D Area	MDBL Area	OES2D Area
Australopithecus anamensis	KNM-KP 29286	m1	115.3	226.7	148.9	129.3
Australopithecus anamensis	KNM-KP 29286	m2	160.6	279.6	198.8	168.7
Australopithecus anamensis	KNM-KP 29286	m3	148.5	255.9	193.7	159.3
Homo erectus	Sangiran 1B	m1	114.5	265.4	169.0	141.6
Homo erectus	Sangiran 1B	m2	128.3	277.7	180.8	153.9
Homo erectus	Sangiran 1B	m3	120.7	253.7	180.0	147.2
Homo neanderthalensis	Scladina 4A I	m1	73.9	216.1	124.0	102.4
Homo neanderthalensis	Scladina 4A I	m2	84.0	211.1	128.3	106.3
Homo neanderthalensis	Scladina 4A I	m3	80.5	189.2	126.5	102.3
Paranthropus boisei	KNM-ER 15930	m1	125.6	281.8	181.9	154.0
Paranthropus boisei	KNM-ER 15930	m2	164.6	320.2	244.2	201.8
Paranthropus boisei	KNM-ER 15930	m3	176.7	342.3	277.5	220.0
Paranthropus robustus	DNH 8	m1	125.8	316.0	215.9	185.5
Paranthropus robustus	DNH 8	m2	150.9	317.4	242.8	203.0
Paranthropus robustus	DNH 8	m3	163.1	370.0	304.3	243.7
Paranthropus robustus	SK 6	m1	162.0	352.7	246.2	207.3
Paranthropus robustus	SK 6	m2	190.7	373.6	286.9	234.2
Paranthropus robustus	SK 6	m3	200.4	374.5	301.3	245.3

Supplementary Table 8 | Results for multiple linear regression of proportion of maximum in tooth row (PropRowMaxP) vs tooth position (ToothNoP) and area of m1 (AreaM1) for *Homo* species.

Plane A

```
Coefficients:
             Estimate Std. Error t value Pr(>|t|)
(Intercept)  0.4405763  0.0940624   4.684 0.000352 ***
ToothNoP     0.2377533  0.0134270  17.707 5.56e-11 ***
AreaM1      -0.0016578  0.0006297  -2.633 0.019684 *
---
Signif. codes:  0 ‘***’ 0.001 ‘**’ 0.01 ‘*’ 0.05 ‘.’ 0.1 ‘ ’ 1

Residual standard error: 0.04591 on 14 degrees of freedom
  (14 observations deleted due to missingness)
Multiple R-squared:  0.9593,     Adjusted R-squared:  0.9535
F-statistic:   165 on 2 and 14 DF,  p-value: 1.848e-10
```

Plane B

```
Coefficients:
             Estimate Std. Error t value Pr(>|t|)
(Intercept)  1.2257523  0.1115384  10.990 2.86e-07 ***
ToothNoP    -0.0821669  0.0207012  -3.969   0.0022 **
AreaM1       0.0006890  0.0004452   1.548   0.1500
---
Signif. codes:  0 ‘***’ 0.001 ‘**’ 0.01 ‘*’ 0.05 ‘.’ 0.1 ‘ ’ 1

Residual standard error: 0.03873 on 11 degrees of freedom
  (10 observations deleted due to missingness)
Multiple R-squared:  0.6226,     Adjusted R-squared:  0.554
F-statistic: 9.075 on 2 and 11 DF,  p-value: 0.004701
```

Supplementary Table 9 | Results for multiple linear regression of proportion of maximum in tooth row (PropRowMaxP) vs tooth position (ToothNoP) and area of m1 (AreaM1) for australopithecines.

Plane A

```
Coefficients:
             Estimate Std. Error t value Pr(>|t|)
(Intercept) 8.096e-02  7.664e-02   1.056    0.309
ToothNoP    2.304e-01  1.652e-02  13.950 1.32e-09 ***
AreaM1      2.379e-06  3.358e-04   0.007    0.994
---
Signif. codes:  0 ‘***’ 0.001 ‘**’ 0.01 ‘*’ 0.05 ‘.’ 0.1 ‘ ’ 1

Residual standard error: 0.0576 on 14 degrees of freedom
  (17 observations deleted due to missingness)
Multiple R-squared:  0.9345,     Adjusted R-squared:  0.9251
F-statistic:  99.8 on 2 and 14 DF,  p-value: 5.197e-09
```

Plane B

```
Coefficients:
             Estimate Std. Error t value Pr(>|t|)
(Intercept) 0.9062316  0.0813763  11.136 5.09e-08 ***
ToothNoP    0.0096313  0.0162932   0.591    0.565
AreaM1      0.0001680  0.0002022   0.831    0.421
---
Signif. codes:  0 ‘***’ 0.001 ‘**’ 0.01 ‘*’ 0.05 ‘.’ 0.1 ‘ ’ 1

Residual standard error: 0.03259 on 13 degrees of freedom
  (10 observations deleted due to missingness)
Multiple R-squared:  0.07408,    Adjusted R-squared:  -0.06837
F-statistic: 0.5201 on 2 and 13 DF,  p-value: 0.6064
```

Supplementary Table 10 | Results for multiple linear regression of proportion of maximum in tooth row (PropRowMaxP) vs tooth position (ToothNoP) and area of m1 (AreaM1) for great apes.

Plane A

```
Coefficients:
             Estimate Std. Error t value Pr(>|t|)
(Intercept)  0.1729463  0.0432668   3.997  0.00312 **
ToothNoP     0.2677833  0.0135136  19.816 9.85e-09 ***
AreaM1      -0.0007271  0.0002288  -3.178  0.01121 *
---
Signif. codes:  0 ‘***’ 0.001 ‘**’ 0.01 ‘*’ 0.05 ‘.’ 0.1 ‘ ’ 1

Residual standard error: 0.03822 on 9 degrees of freedom
  (10 observations deleted due to missingness)
Multiple R-squared:  0.9781,     Adjusted R-squared:  0.9733
F-statistic: 201.4 on 2 and 9 DF,  p-value: 3.374e-08
```

Plane B

```
Coefficients:
             Estimate Std. Error t value Pr(>|t|)
(Intercept)  1.2875205  0.1459685   8.821 0.000311 ***
ToothNoP    -0.0836563  0.0307087  -2.724 0.041567 *
AreaM1       0.0003374  0.0003184   1.060 0.337646
---
Signif. codes:  0 ‘***’ 0.001 ‘**’ 0.01 ‘*’ 0.05 ‘.’ 0.1 ‘ ’ 1

Residual standard error: 0.04343 on 5 degrees of freedom
  (10 observations deleted due to missingness)
Multiple R-squared:  0.6309,     Adjusted R-squared:  0.4832
F-statistic: 4.272 on 2 and 5 DF,  p-value: 0.08279
```

References